

CHALMERS



Influence of Cracks on Chloride-Induced Corrosion in Reinforced Concrete Structures

Master's Thesis in the International Master's Programme Structural Engineering

NHAN THE TRAN

QI HUANG

Department of Civil and Environmental Engineering

Division of Structural Engineering

Concrete structures

CHALMERS UNIVERSITY OF TECHNOLOGY

Gothenburg, Sweden 2006

Master's Thesis 2006:40

MASTER'S THESIS 2006:40

Influence of Cracks on Chloride-Induced Corrosion in Reinforced Concrete Structures

Master's Thesis in the International Master's Programme Structural Engineering

NHAN THE TRAN

QI HUANG

Department of Civil and Environmental Engineering
Division of Structural Engineering
Concrete structures
CHALMERS UNIVERSITY OF TECHNOLOGY
Gothenburg, Sweden 2006

Influences of Cracks on Chloride-induced Corrosion in Reinforced Concrete Structures

Master's Thesis in the International Master's Programme Structural Engineering

NHAN THE TRAN

QI HUANG

© NHAN THE TRAN & QI HUANG, 2006

Master's Thesis 2006:40

Department of Civil and Environmental Engineering

Division of Structural Engineering

Concrete structures

Chalmers University of Technology

SE-412 96 Gothenburg

Sweden

Telephone: + 46 (0)31-772 1000

Cover: Photo of concrete beams with load on in Chalmers laboratory

Chalmers Reproservice / Department of Civil and Environmental Engineering
Gothenburg, Sweden 2006

Influence of cracks on Chloride-induced corrosion in concrete structures
Master's Thesis in the International Master's Programme Structural Engineering
NHAN THE TRAN
QI HUANG
Department of Civil and Environmental Engineering
Division of Structural Engineering
Concrete structures
Chalmers University of Technology

ABSTRACT

Corrosion of reinforcement is a major problem for the durability of reinforced concrete structures. Generally, reinforcement corrosion is caused by carbonation or chlorides. Earlier studies have mainly been focused on the influence of carbonation or chlorides on corrosion in uncracked concrete structures. The aim of the thesis was to investigate the influence of cracks on reinforcement corrosion, especially chloride-induced corrosion. Furthermore, a test method was developed by the authors to investigate this matter.

In the first part of the report, literature studies of the corrosion process and influence of cracks on reinforcement corrosion are presented. Reinforcement corrosion process was influenced by many factors such as relative humidity, temperature.

In the second part, experiments were carried out to investigate the influence of cracks on the initiation and propagation of reinforcement corrosion process. Especially, their effect on the initiation period of chloride-induced corrosion was studied. Three groups of concrete beams were cast. The beams in group A were loaded to cracking, and the load was kept during the test. The beams in group B were loaded to cracking, and thereafter unloaded. The beams in the group C were considered as a reference group which were not loaded, and thus uncracked. All the beams in the three groups were exposed to salt water. Small concrete covers (20mm) and a high concentrated salt in the solutions (10%) were used in order to get reinforcement corrosion in a limited time. Half cell potential measurements were used to investigate when corrosion of the reinforcement started.

The results of the experiments show that reinforcement corrosion started already after about 2 weeks in group A and about 3-4 weeks in group B. However, reinforcement corrosion did not start after 12 weeks exposure of the specimens in group C. Thus, the results indicated that the presence of cracks strongly influences the initiation time for reinforcement corrosion, but also the width of the cracks influences initiation.

Key words: crack, half cell potential, corrosion, carbonation, chloride-induced, initiation period, propagation period

Contents

1	INTRODUCTION	5
1.1	Background	5
1.2	Aim and limitations	5
1.3	Outline of the report	5
2	CORROSION PROCESS	6
2.1	General description	6
2.1.1	Overview of corrosion due to carbonation and crack	6
2.1.2	Overview of corrosion due to chloride and crack	8
2.2	Initiation and propagation period	9
2.3	Factors influencing the corrosion	10
2.3.1	Moisture conditions	10
2.3.2	Temperature	11
2.3.3	Water-cement ratio	13
2.3.4	Cement type	14
2.4	Corrosion measurement	16
2.4.1	Visual inspection	16
2.4.2	Carbonation depth measurement	17
2.4.3	Chloride measurement	18
2.4.4	Half cell potential measurement	19
2.4.5	Resistivity measurement	21
2.4.6	Linear polarisation	22
3	INFLUENCE OF CRACKS ON CHLORIDE INDUCED CORROSION	25
3.1	Types of crack	25
3.1.1	Cracks due to load (static and/or dynamic)	25
3.1.2	Cracks due to shrinkage	27
3.1.3	Cracks due to temperature	28
3.1.4	Cracks due to corrosion	29
3.1.5	Other types of cracks	29
3.2	Influence of cracks in the initiation period	31
3.3	Influence of cracks in the propagation period	32
4	REVIEW OF EXISTING TESTS ON THE INFLUENCE OF CRACKS ON CHLORIDE INDUCED CORROSION	34
4.1	Experiment by Francois	34
4.1.1	Purpose	34
4.1.2	Reinforced concrete sample	34
4.1.3	Loading and exposure conditions	35
4.1.4	Measurements	36
4.1.5	Results	36

4.2	Experiment by Mohammed	37
4.2.1	Purpose	37
4.2.2	Reinforced concrete sample	37
4.2.3	Loading and exposure conditions	37
4.2.4	Measurements	39
4.2.5	Results	39
5	EXPERIMENTS	40
5.1	Introduction	40
5.2	Test specimens	40
5.3	Loads	42
5.4	Crack widths	44
5.5	Exposure conditions	45
5.6	Measurements	46
5.6.1	Half cell potential measurements	46
5.6.2	Corrosion rate measurement	48
5.6.3	Destructive measurement	48
5.7	Results	50
5.7.1	Half cell potential results	50
5.7.2	Destructive results	56
6	CONCLUSIONS AND SUGGESTIONS FOR FURTHER RESEARCH	58
7	REFERENCES	61
	APPENDIX A: CEMENT TYPES IN PARROTT'S RESEARCH	64
	APPENDIX B: RECORD OF POTENTIAL MEASUREMENT	65
	APPENDIX C: DESIGN CALCULATION FOR LOAD AND CRACK WIDTHS	72
	APPENDIX D: ACTUAL COMPRESSIVE STRENGTH	74
	APPENDIX E: COMPARISON BETWEEN COUNT/GUARD AND SILVER/SILVER CHLORIDE ELECTRODE IN ELECTRICAL POTENTIAL MEASUREMENT	75
	APPENDIX F: RELATION BETWEEN MASS LOSS OF REINFORCEMENT BARS AND CLEANING CYCLES	76

Preface

This thesis is submitted as a partial fulfilment of the requirements for the International Master Degree. The study was carried out from October 2005 until April 2006 at Chalmers University of Technology, at the department of Civil and Environmental Engineering, Division of Structural Engineering, Concrete Structures. All the experiments were performed at Building Technology Division laboratory, Chalmers, Gothenburg, Sweden.

At first, we would like to thank our supervisors, PhD Anders Lindvall, PhD and Associate Prof. Karin Lundgren, who was also the examiner, for their encouraging support and inspiration throughout the work. We would also thank Marek Machowsky and Tang Luping for their assistance in the laboratory work. We would like to give our appreciation to Ulrika Nyström, our opponent, for her comments on the project and all good moments we have had together.

Furthermore, we would like to express our gratitude to all staff at the Division of Structural Engineering. Special thanks to Björn Engström for the concrete knowledge we received during courses, for the well organized master program in structural engineering, and for his general guidance and kindness during our study at Chalmers.

Last but not least, we take the opportunity to express our ever lasting love to our family and friends for their never ending supports.

Gothenburg April 2006

NHAN THE TRAN

QI HUANG

1 Introduction

1.1 Background

Reinforced concrete is an economical and successful construction material. It is usually durable and strong, performing well during its service life. However, corrosion of the reinforcement is a major problem for the durability of reinforced concrete structures. Normally, reinforcement corrosion is caused by carbonation and chloride ingress. Reinforcement corrosion can be divided into two periods. In the initiation period, carbon dioxide and/or chloride ions are transported through the concrete cover, eventually reach and break down the protective layer of the steel. Thereafter, in the propagation period, corrosion products form in the reinforcement. Cracks can occur in concrete structures due to a lot of reasons, for examples, load and reinforcement corrosion. Once cracks take place, they will influence the reinforcement corrosion process.

1.2 Aim and limitations

The aim of the thesis was to investigate the influence of cracks and external load on the reinforcement corrosion process. Especially, their effect on the initiation period of chloride-induced corrosion was studied. Experiments were designed to test this. The work was limited by investigation of certain external static load and crack widths.

1.3 Outline of the report

The first part of the thesis is a literature study, including a general description of the reinforcement corrosion process, factors influencing reinforcement corrosion, the influence of cracks and load on reinforcement corrosion, and methods to measure reinforcement corrosion. The second part of the thesis describes experiments carried out by the authors to further investigate the influence of cracks on reinforcement corrosion. Some conclusions and recommendations for future research are also given. All the corrosion in the thesis is reinforcement corrosion.

2 Corrosion Process

2.1 General description

Good quality reinforced concrete structures normally have excellent chemical protection for reinforcement against corrosion due to high alkalinity and low permeability of the concrete cover. At the beginning, the concrete surrounding the reinforcement is highly alkaline with a pH value between 13 and 14. As a result, the interaction between reinforcement and hydroxyl ions creates the formation of an insoluble ferric oxide, which causes the steel to be passivated. However, the high alkalinity or the low permeability of the cover will not guarantee permanently that the steel will resist corrosion. Reinforcement corrosion is caused by two main reasons: carbonation and chloride ingress.

The mechanism for corrosion is based on anode and cathode reactions in an electrolyte. Corrosion takes place at the anode with the release of hydrogen gas or the formation of hydroxyl ions at the cathode. These hydroxyl ions may react with metal ions dissolved at the anode and form metal hydroxides or hydrated oxides.

Thus, reinforcement corrosion needs three general requirements to start:

- Difference in potential on reinforcement rebar
- Electrolyte
- Oxidizing agent

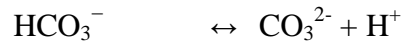
2.1.1 Overview of corrosion due to carbonation and crack

In the case of carbonation, chemical reaction between carbon dioxide, CO₂ from the air and the hydration products of cement in concrete causes a reduction in the alkalinity of concrete, thus the pore solution, which surrounds steel is neutralised. pH in concrete is decreased from 13 or 14 to levels below 9. At low pH, concrete loses its protective nature, thereafter, when the embedded steel is exposed to oxygen and ion bearing solution, corrosion of the reinforcement commences. Neutralisation can also occur besides carbonation. However, carbonation is the dominating neutralisation mechanism for concrete in air.

Carbonation can simply be defined as the reaction of carbon dioxide, CO₂ with calcium hydroxide, Ca(OH)₂ in the hardened cement paste, resulting in the production of calcium carbonate, CaCO₃. This reaction occurs as follows:



Carbon dioxide also dissolves in concrete pore water and forms carbonic acid before reacting with the dissolved Ca(OH)_2



The following neutralization reaction completes the final stage of carbonation



Reaction (3) shows that carbonation consumes Ca(OH)_2 , a product which endows concrete with high pH. The rates of the reactions (1) and (3) play an important role in the carbonation of concrete, Isgor *et al.* (2002).

When pH is reduced to 8.5~9.0, the passivation layer of reinforcement is destroyed and then the reinforcement will start to corrode. One kind of this reaction occurs as follows:



The volume of the rust product is 2~4 times larger than the original steel it was formed of. This causes compression to concrete, and can lead to splitting cracks in the concrete cover.

In many cases, after crack happens, it is easier for the water and oxygen to go inside of the cracks to the reinforcement which will increase the corrosion rate of reinforcement. It makes carbon dioxide, CO_2 easier to react with calcium hydroxide, Ca(OH)_2 after crack happens. These will make the passivating layer around the reinforcement become weaker and weaker. And thus, it increases the corrosion. But carbonation will not increase the corrosion of concrete in some cases, for example, if the cover of concrete is thick enough to prevent the water or oxygen going inside even if the crack happens.

In all, the carbonation depth of concrete is an important index for evaluating the damage and durability of reinforced concrete structures. The carbonation process of concrete structures at cracks consists of four steps: diffusion of CO_2 into the crack, diffusion of CO_2 into the concrete, chemical reaction, and diffusion of hydroxyl ions. The study by Steffens *et al.* (2002) indicates that the carbonation rates of both uncracked and cracked concrete structures follow normal distribution. As regards the

pure process of carbonation, the same basic interrelations given for uncracked concrete are valid for carbonation in the cracked regions as well. Carbonation can penetrate into the interior of cracked concrete much faster than it does through uncracked concrete.

2.1.2 Overview of corrosion due to chloride and crack

When chloride ions enter the concrete during mixing or after exposure in the environment, they depassivate the steel by locally breaking down the protective layer Fe_2O_3 . Chlorides act as catalyst to corrosion when there is sufficient concentration at the rebar surface. They are not consumed in the process but help to break down the passive layer and allow the corrosion process to proceed quickly. This is illustrated in Figure 2.1

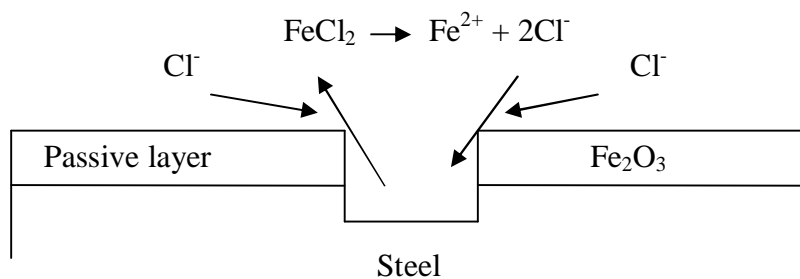


Figure 2.1 The break down of the passive layer, Broomfield (1997)

Before chloride initiated corrosion can take place in concrete, a certain amount of chloride must be present near the steel surface. This amount is generally referred to as the chloride threshold level. The chloride threshold level is not a single value valid for all types of concretes, steels and environments, but it is affected by a number of different factors such as cover thickness, temperature and so on, Nilsson *et al.* (1996).

Similar to carbonation process, when rust product is formed, they cause cracks in the cover of reinforced concrete structure. The influence of cracks on the chloride induced process will be discussed in chapter 3.2 and 3.3.

2.2 Initiation and propagation period

From the view of reinforcement corrosion, the service life of reinforced concrete structures is divided into an initiation and a propagation period (see Figure 2.2). The initiation period is the time for carbon dioxide and/or chloride ions to reach and break down the protective layer of the steel.

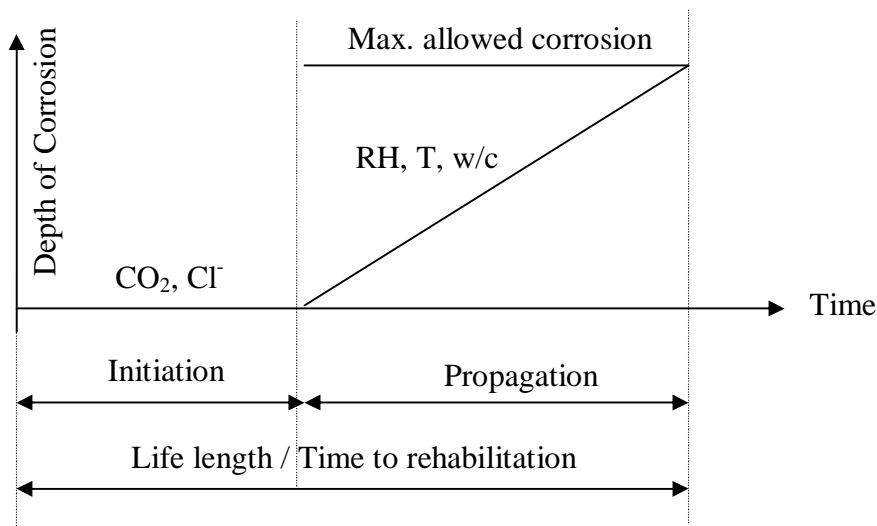


Figure 2.2 Model of reinforcement corrosion. (The model is applied to homogenous and uncracked concrete with standard reinforcement), Tuutti (1982)

The propagation period starts when corrosion products begin to form in the reinforcement. The inclination of the line in the propagation area gives the corrosion rate. When the maximum allowed corrosion is reached, the structure needs to be rehabilitated.

Some of the parameters that are influencing the initiation period and the propagation period are listed below:

- The thickness of the concrete cover
- Moisture and relative humidity (RH) in the cover and at the reinforcement
- Temperature (T), CO₂, Cl⁻
- Water cement ratio (w/c)
- Cement type

2.3 Factors influencing the corrosion

2.3.1 Moisture conditions

The moisture content in concrete is highly influenced on the initiation time for reinforcement corrosion as it delays the intrusion of carbon dioxide but is a prerequisite for the penetration of chlorides. In the propagation period, the rate of corrosion is also influenced by moisture. The rate is slow in dry or wet condition but in-between moisture acts as an electrolyte and allows the intrusion of oxygen to the corrosion process, DuraCrete (1999).

Moisture plays a significant role in chemical reactions in concrete and in parts of physical processes in concrete. The rate of reaction between a solid and a gas, such as carbonation in rather dry concrete, will be affected to a certain extent by moisture at low relative humidity (RH). Relative humidity is the ratio of the actual vapour concentration of water to the saturation vapour concentration at that temperature. The effects of the moisture conditions on the rates of reaction are shown in Figure 2.3.

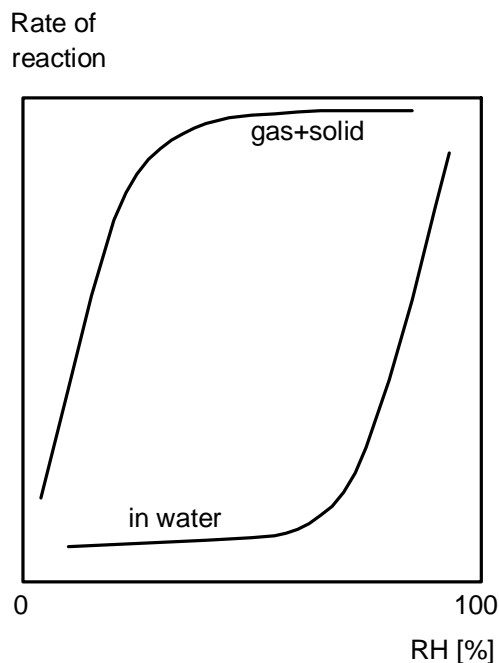


Figure 2.3 The relation between moisture conditions and rates of reaction Nilsson (1980), Tuuti (1982), Goodbrake et al (1979) and Nilsson & Peterson (1983).

Moisture will be an obstacle to gas and vapour flow in the pore system of a concrete but a prerequisite for the movement and penetration of ions. The relation between moisture conditions and flow rate is described in Figure 2.4.

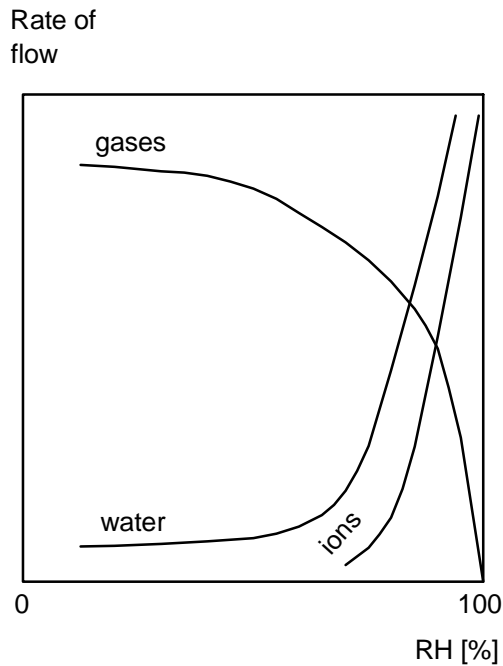


Figure 2.4 The relation between moisture conditions and rates of reaction Nilsson (1980), Tuuti (1982), Goodbrake *et al* (1979) and Nilsson & Peterson (1983)

RH in the pores is not simply related to atmospheric RH. Water splash, run off or capillary action, formation of dew, solar heat gain or other factors may intervene. RH influences how much water there is in the pores, which in turn affects the corrosion process and transport of different matters. Outdoor structures normally have fairly high RH in the pore system. Chloride induced corrosion is at a maximum when the RH within the concrete is around 90-95%, Tuutti (1982). For carbonation, there was experimental evidence that the peak is around 95-100% RH, Broomfield (1997).

2.3.2 Temperature

Laboratory tests have shown that the chloride levels in extracted pore fluid from chloride exposed cement paste were lower at low temperatures than at higher temperatures, Larsson *et al.* (1995). Examination of concrete exposed to sea water in Greenland shows a very high chloride content at the concrete surface, Nilsson *et al.* (1996).

In reinforced concrete structures, the higher the temperature (T), the higher the corrosion rate. Maslehuddin *et al.* (1996) showed that when concrete was mixed with Ordinary Portland Cement, an increase in corrosion rate with temperature was observed, see Figure 2.5. The corrosion rate on steel in reinforced concrete exposed at

15 to 40°C increased slightly. The values increased rapidly when the temperature was over 40°C.

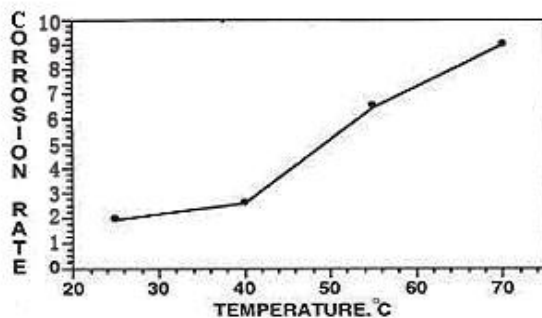


Figure 2.5 Effect of temperature on corrosion rate in OPC-A concrete, Maslehuddin et al. (1996)

For reinforced concrete with another Ordinary Portland Cement, OPC-B ($C_3A = 14.5\%$), the effect of temperature on corrosion rate is plotted in Figure 2.6. The experiment indicated an increase in corrosion activity with exposure temperature.

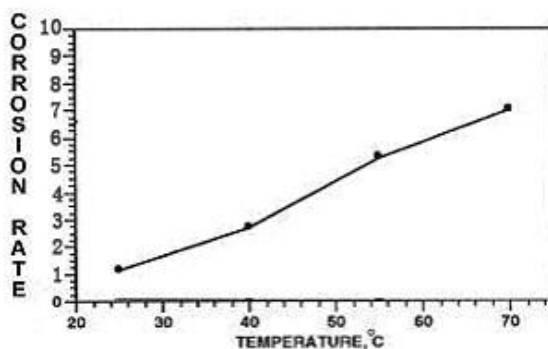


Figure 2.6 Effect of temperature on corrosion rate in OPC-B concrete, Maslehuddin et al. (1996)

For reinforced concrete, which uses Sulphate Resisting Portland Cement (SRPC), containing 3.5% of C_3A , the corrosion rate approximately doubled when the temperature changed from 25 to 70°C, see Figure 2.7.

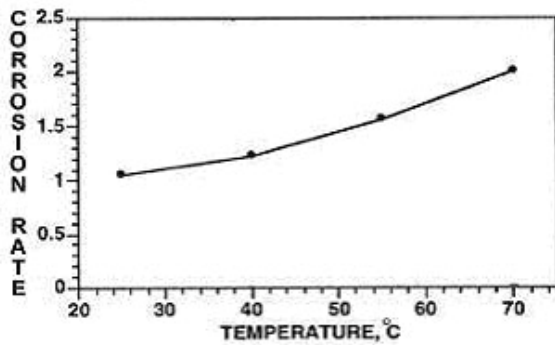


Figure 2.7 Effect of temperature on corrosion rate in SRPC concrete, Maslehuddin et al. (1996)

The data in Figure 2.5 to 2.7 indicate that the corrosion rate of the reinforcement was affected by the temperature. The corrosion activity increased by 2 to 6 times due to an increase in the temperature from 25 to 70°C, the acceleration factor for every 15°C being in the range of 1.26 to 1.87. This may be attributed to an increase in the rate of chemical reactions.

2.3.3 Water-cement ratio

The higher the water-cement ratio, the more negative will the effect on reinforcement corrosion be. For concrete containing ordinary Portland cement, time to initiate the corrosion drops from 90 to 20 days when the ratio increases from 0.4 to 0.6. The effect includes a faster diffusion of chloride ions into the steel surface, easier oxygen penetration and lower electrical resistivity. The negative effect of increasing the w/c ratio on the time to initiate corrosion is shown in Figure 2.8.

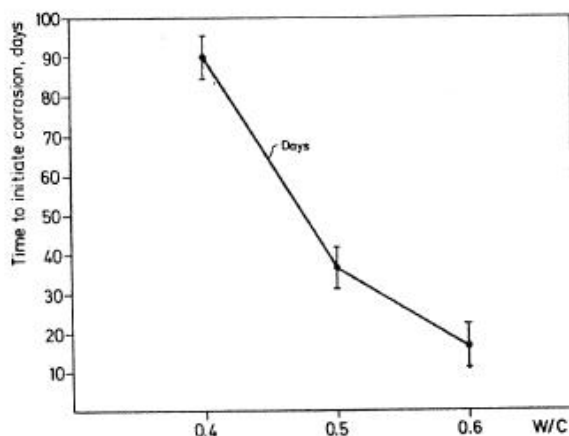


Figure 2.8 The effect of w/c ratio on ordinary Portland cement samples on the time required to initiate corrosion, Pettersson (1992)

In concrete under a moist environment, the cathodic reaction rate depends on the oxygen permeation quantity and the corrosion rate is limited by the cathodic reaction, Otsuki *et al.* (2000). With the decrease in the w/c, the quantity of oxygen permeation decreased. Therefore, decreasing the w/c restrained the cathodic reaction, which leads to a decrease in the corrosion rate. In addition, the concrete resistance increased with a decrease in the w/c. As a result, the corrosion rate decreased with a decrease in the w/c. Moreover, the corrosion rate may also be controlled by the concentration of alkalinity, which will naturally be higher in the concrete that has a lower w/c, the corrosion rate slowed down in case of low water cement ratio. The results of the influence of w/c on the total corrosion rate are shown in Figure 2.9.

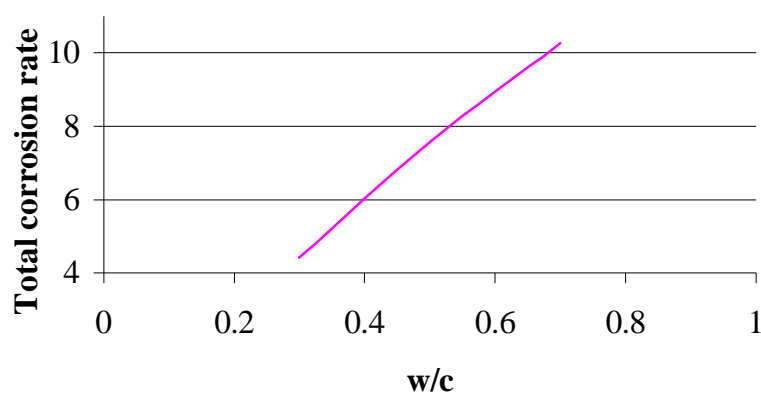


Figure 2.9 Influence of w/c ratio on the total corrosion rate, Otsuki *et al.* (2000)

2.3.4 Cement type

Cement type is another factor that influences the corrosion. Experiments to analyse the effect of cement types on chloride-induced reinforcement corrosion were conducted by Parrott (1996). The experiments were carried out with different cement types. These cement types contained different amount of ground granulated blastfurnace slag (GGBS) and limestone. Details of these cement types are given in appendix A.

The effect of cement on corrosion rate in similar exposure conditions is plotted in Figure 2.10. The results showed that the highest rate of corrosion was in reinforced concrete containing cement type F7. High corrosion rate was observed for cement type U7, U8 and F4. Low corrosion rate was in cement type F1, U5; U3.

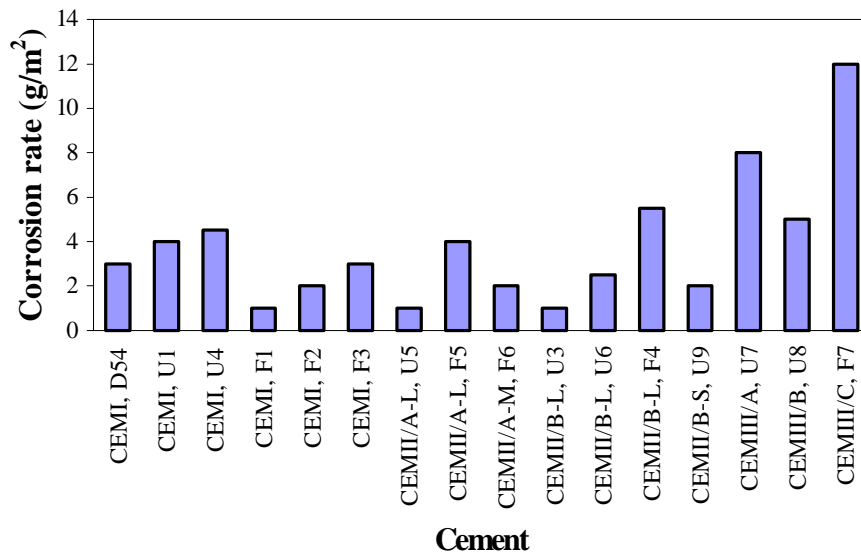


Figure 2.10 Effect of cement on chloride induced corrosion, 20-mm concrete cover, Parrott (1996)

2.4 Corrosion measurement

A full evaluation of the condition of corroding reinforced concrete structures is normally a two-stage process. The preliminary measurement characterises the nature of the corrosion and gives guidance in planning a detailed measurement. This normally involves a visual inspection, probing of cracks and spalls to see their extent. The detailed measurement will confirm the cause and quantify the extent of corrosion. This stage will show how much damage that has occurred and what has caused the damage. Table 2.2 lists most of the techniques that can be used for corrosion measurements and what they detect.

Table 2.2 Corrosion measurements

Measurement	Detects
Visual inspection	Surface defects
Carbonation depth	Carbonated depth
Chloride content	Chloride ingress
Half cell potential	Probability of corrosion
Resistivity	Concrete resistivity
Linear polarization	Corrosion rate

2.4.1 Visual inspection

Visual inspection is the first step in an investigation. The aim of the visual survey is to give a first indication of what is wrong and how extensive the damage is. If the concrete is spalling, that can be used as a measure of extent of damage. A visual inspection should include the following parameters in Table 2.3:

Table 2.3 Visual inspection – simplified defect classification

Feature	Description	Cause	Details
Cracking	Jagged separation of concrete	Overload, corrosion, shrinkage	Direction, width, depth
Rust stains	Brown stains	Corrosion of steel, tying wire or surface steel work	Area
Spall	A fragment detached from a larger mass	Exertion of internal pressure due to rebar corrosion or external force	Area, depth

The interpretation of the results is based on the experience of the technicians conducting the survey. Visual survey should be followed up by testing to confirm the cause of corrosion.

2.4.2 Carbonation depth measurement

Equipment and use

Carbonation can be measured by exposing fresh concrete and spraying it with phenolphthalein. It is the most reliable, convenient and widely used indicator. The phenolphthalein indicator will remain clear when concrete is carbonated and will turn to pink when concrete is alkaline. The indicator can be 1g per 100ml of alcohol/water, 50:50 mix, Broomfield (1997). To increase the accuracy measurement, the sample should be prepared carefully to prevent dust from carbonated areas contaminating the un-carbonated surface.

Interpretation

If carbonation front does not run as a straight line parallel to the surface, Figure 2.11(1), the depth of the carbonation will be determined in the following way, NORDTEST (1989)

- In case of the carbonation front running as in Figure 2.11 (2), a graphical average and the maximum is to be recorded.
- In case of the carbonation front running as in Figure 2.11 (3), the maximum depth of carbonation is to be recorded as well as normal depth.

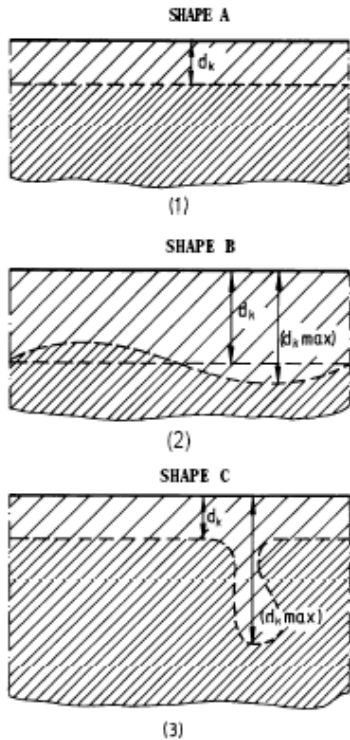


Figure 2.11 Defining the depth of carbonation according to shape, NORDTEST (1989)

2.4.3 Chloride measurement

Equipment and use

Chlorides are usually measured by dissolving powder samples in acid. The samples are taken from drilling or crushed cores. The cores are collected at different depths so that the chloride profile can be investigated, in which the relation between chloride by weight of cement and the depth is defined. Then in the laboratory, powdered sample are dissolved in acid, and then analysed to find the total chloride contents.

There are also methods to measure the free chlorides. This refers to the fact that it is the chloride dissolved in the pore water that contributes to the corrosion process. Any chlorides chemically bound up in the cement or bound up in the aggregate do not contribute to the corrosion threshold. The water soluble chloride tests (ASTM D1411, AASHTO T260) are used to measure the free chlorides.

Interpretation

Chloride profiles can be used to determine the diffusion coefficient and thus predict the ongoing rate of ingress. Actually, the chloride level at the rebar determines the present extent of corrosion, but the profile can be used to predict the future rate, as that is what drives more chlorides from the concrete surface in to the steel surface.

2.4.4 Half cell potential measurement

Equipment and use

There are several methods to detect the corrosion. Many of them are electrochemical methods. The half cell potential method is currently the most widely used method for the detection of reinforcement corrosion. The half cell potential method is defined as the voltage difference between the reinforcement and a reference electrode.

The half cell is a simple device. The electrode is a piece of metal in a solution of its own ions, such as copper in copper sulphate, silver in silver chloride etc. A high impedance digital voltmeter is used to collect the data, connecting the electrode and the reinforcement, as Figure 2.12.

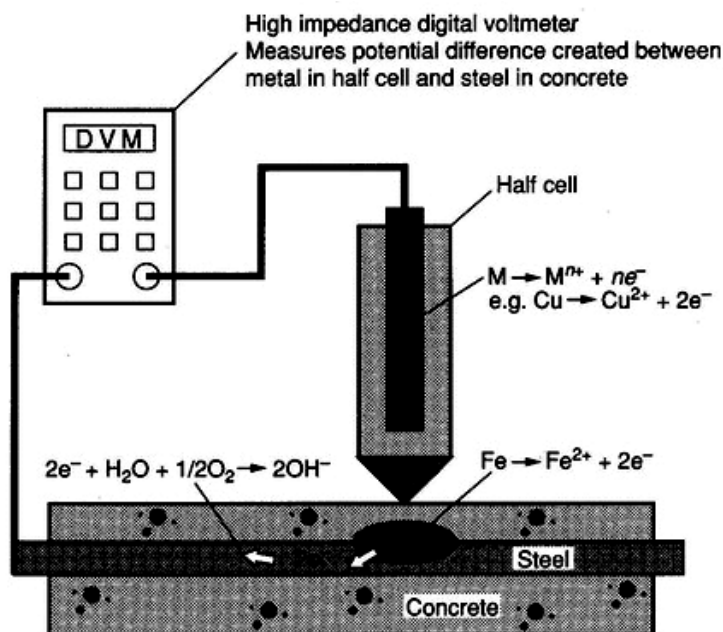


Figure 2.12 Half cell potentials measurement, Broomfield (1997)

The measurement procedure with a half cell is as follows, Broomfield (1997):

- Decide the area of measurement.
- Use a cover meter to locate the steel and determine rebar spacing.
- Make an electrical connection to the steel either by exposing it or using already exposed steel.
- Check that the steel is electrically continuous with a DC resistivity meter between 2 points
- Check and calibrate the half cell and voltmeter.
- Wet the whole area to ensure good electrical contact if necessary. Tap water or soap solution is recommended for wetting.
- Take and record the readings. The readings are recorded if two readings are within few millivolts of each other.
- Check for the most negative reading area for signs of corrosion.

Interpretation

The half cell potential measurement is interpreted in different ways

- Detection of corroding steel bars, the criteria of corrosion is illustrated in Table 2.4.
- Definition of position of additional tests such as corrosion current, chloride profiles, embedding of sensor for monitoring
- Design of and anode layout for cathodic protection or electrochemical repair
- Assessment of corrosion state after repair

Table 2.4 Criteria for corrosion of steel in concrete (ASTM C867)

Cu/CuSO₄ electrode	Ag/AgCl electrode	Corrosion condition
>-200 mV	>-106 mV	Low (10% risk of corrosion)
-200 to -350 mV	-106 to -256 mV	Intermediate corrosion risk
< -350 mV	< -256mV	High (<90% risk of corrosion)
< - 500 mV	< - 406mV	Severe corrosion

2.4.5 Resistivity measurement

Equipment and use

Concrete resistivity in its basic definition is a material property. In practice, measurements are often done by using surface contact electrodes. The simplest method is to apply two electrodes onto the concrete surface and measure the resistivity between them, but the most available tool for real use is the Wenner four-probe tool, Millard *et al.* (1990).

The Wenner four-probe system is shown in Figure 2.13. The current (I) is applied between the two outer probes and the potential difference (V) measured across the two inner probes. This approach eliminates any effects due to surface contact resistances.

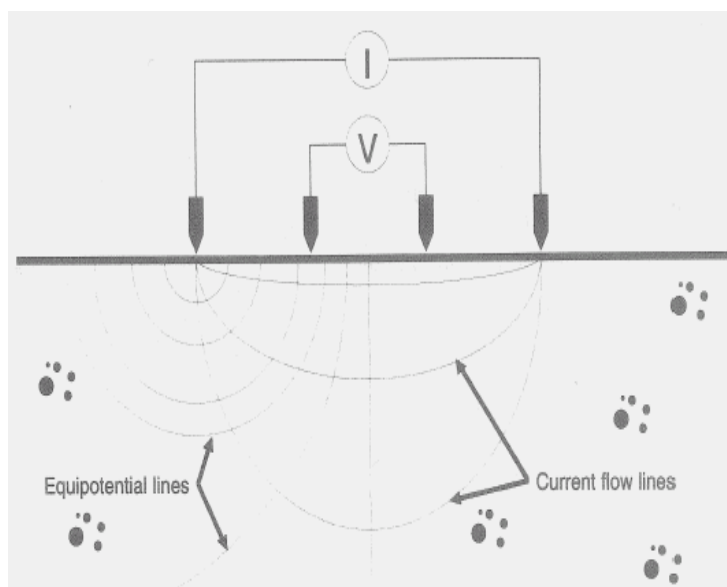


Figure 2.13 The four-probe Wenner-type resistivity measurement, Broomfield (1997)

Interpretation

The resistivity of concrete is an indicator for the risk of early corrosion. Low resistivity of concrete is related to a rapid chloride ingress or high corrosion rate.

Concrete resistivity (R) of the area around the sensor is calculated by an equation:

$$R = 2 \cdot R_{iR} \cdot D$$

Where

R: Resistivity in $k\Omega\text{cm}$

R_{iR} : Resistance between rebar network and electrode $k\Omega$

D: Diameter of electrode, cm

The interpretation of the Wenner four-probe system is as follows

$R > 20 k\Omega\text{cm}$	Low corrosion rate
$10 k\Omega\text{cm} < R < 20 k\Omega\text{cm}$	Low to moderate corrosion rate
$5 k\Omega\text{cm} < R < 10 k\Omega\text{cm}$	High corrosion rate
$R < 5 k\Omega\text{cm}$	Very high corrosion rate

2.4.6 Linear polarisation

Equipment and use

Polarisation resistance is determined by measuring the change in corrosion current induced by a change in corrosion potential. A schematic of the linear polarisation device is shown in the Figure 2.14. It has a control box that applies the current and records the measurement. There are two sensors. Sensor A is used to measure corrosion potential (E_{corr}) and applied current (I) and the other one is used to measure temperature and relative humidity.

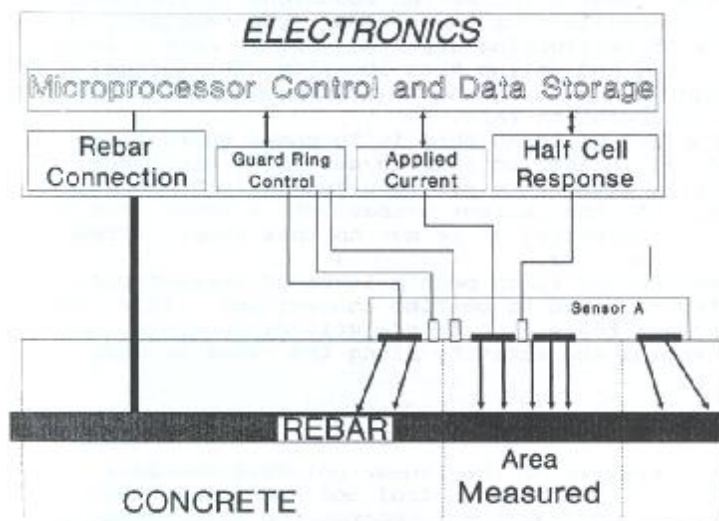


Figure 2.14 Schematic of corrosion rate device showing sensor A, Broomfield (1997)

The linear polarisation device applies a small electrical current ΔI and measures the shift in potential ΔE . The ratio $\Delta E/\Delta I$ is called the polarisation resistance R_p . The polarisation resistance is inversely proportional to the corrosion current I_{corr} .

$$R_p = \Delta E/\Delta I$$

$$I_{corr} = B/R_p$$

where B is a constant, varying from 26 to 52mV depending on the passive or active condition of the steel.

Interpretation

The major advantage of the technique is to estimate the instant rate of uniform corrosion. Classification of corrosion rates is given in Tables 2.5 and 2.6

Table 2.5 Interpretation of measurements. Rodriugiez et al. (1994)

Current density (mA/cm ²)	Average corrosion (Uniform corrosion) (mm/year)	Corrosion rate
<0.1 - 0.2	<1.2 - 2.3	Passive condition
0.2 - 0.5	2.3 - 5.8	Low to moderate
0.5 - 1.0	5.8 - 11.6	Moderate to high
>1.0	>11.6	High

Table 2.6 Interpretation of measurements. Millard (1993)

Current density (mA/cm ²)	Average corrosion (General corrosion) (mm/year)	Corrosion rate
<0.1	<1	Passive condition
0.1 - 1	1-10	Low to moderate
1- 10	10-100	Moderate to high
10 -100	100-1000	High

Pitting corrosion will influence the accuracy of a corrosion rate measurement. If pitting is occurring then the corrosion current is not coming from the whole of the surface area under test. The rate of corrosion penetration within the pit is therefore very high, approximately five to ten times as high as that found for general corrosion.

3 Influence of cracks on chloride induced corrosion

Chloride ion transport in concrete has been investigated over many years. However, most of these studies assume uncracked concrete. In fact, most of concrete structures are designed as reinforced concrete elements that are expected to be cracked already in the serviceability limit state. Thus, the presence of cracks can function as a transport way for chlorides.

3.1 Types of crack

Cracking occurs over time in virtually all concrete. Cracking can not be prevented but it can be significantly reduced or controlled when the causes are taken into account and preventative steps are taken. There is a wide range of crack types, each depending on the lifetime and phase of the concrete. The basic types of cracks are those cracks due to load, shrinkage, temperature and corrosion.

3.1.1 Cracks due to load (static and/or dynamic)

Crack types due to load are as follows:

- Flexural cracks. When bending moment is applied in a structure, it creates tensile stress. If tensile stress is more than tensile strength of concrete, cracks can occur as Figure 3.1

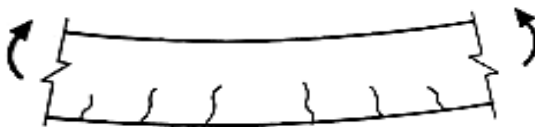


Figure 3.1 Flexural cracks, Engström (2004)

- Tensile cracks. Similar to bending, when tensile stress due to tension is larger than tensile strength, cracks will take place as Figure 3.2

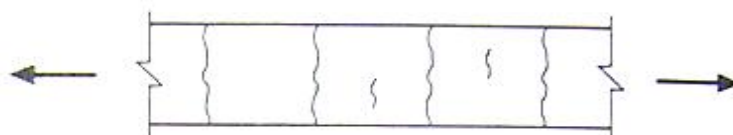


Figure 3.2 Tensile cracks, Engström (2004)

- Shear cracks. When principal tensile stress in the web is higher than tensile strength, web shear cracks appear as Figure 3.3

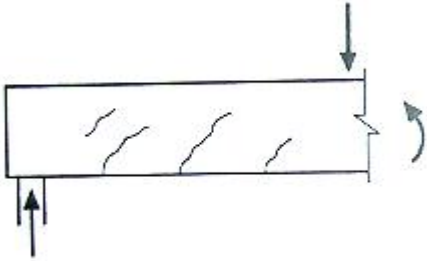


Figure 3.3 Shear cracks, Engström (2004)

- Torsion cracks: Cracks due to torsion applied in the structures as Figure 3.4

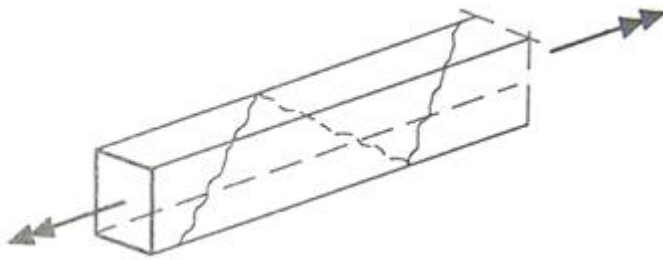


Figure 3.4 Torsion cracks, Engström (2004)

- Splitting crack under concentrated loads: Cracks due to concentrated loads as Figure 3.5

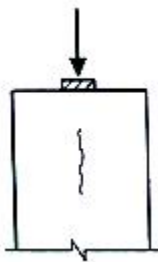


Figure 3.5 Splitting crack under concentrated loads, Engström (2004)

3.1.2 Cracks due to shrinkage

Cracks due to drying shrinkage

In order to obtain concrete with a good workability, almost all concrete is mixed with more water than is needed in the hydration process. However, much of the remaining water will evaporate. Then it will cause the concrete to shrink. Tensile stresses which cause concrete cracking will develop in the hardened concrete due to restraint to shrinkage. This type of cracks is shown in Figure 3.6.



Figure 3.6 Cracks due to drying shrinkage, Portland cement association (2005)

Cracks due to plastic shrinkage

Plastic shrinkage cracking is caused by the rapid loss of water from the surfaces of the fresh concrete. The cracks form when the rate of evaporation is greater than the concrete's bleeding rate. With the loss of water from the concrete surface, there is a volumetric contraction of the fresh concrete. The shrinkage occurs primarily in the paste, with the aggregate acting only as restraint. These differential volume changes can induce tensile stresses in the concrete, and can subsequently cause cracks to form. The fresh concrete does not have sufficient strength to resist these capillary stresses within the fresh paste. This type of cracks is shown in Figure 3.7.



Figure 3.7 Cracks due to plastic shrinkage, Portland cement association (2005)

3.1.3 Cracks due to temperature

Temperature rise results from the heat of hydration of cementitious materials. Tensile stresses are caused when the surface concrete is cooling and contracting, while the interior concrete increases in temperature and expands. If the temperature differential between the surface and center is too great, thermal cracks will be caused due to the tensile stress. The width and depth of cracks depends upon the temperature differential, physical properties of the concrete, and the reinforcing steel. This type of cracks is shown in Figure 3.8.



Figure 3.8 Cracks due to temperature, Portland cement association (2005)

3.1.4 Cracks due to corrosion

Corrosion of reinforcing bars produces rust, which occupies significantly more space than the original metal, and causes expansive forces within the concrete. Cracking and spalling are frequent results. This type of cracks is shown in Figure 3.9.



Figure 3.9 Cracks due to corrosion, Portland cement association (2005)

3.1.5 Other types of cracks

Settlement cracks

Settlement cracking results from insufficient consolidation (vibration), high slumps (overly wet concrete), or a lack of adequate cover over embedded items. Settlement cracks may develop over embedded items, such as reinforcing steel, or adjacent to forms or hardened concrete as the concrete settles or subsides.

Alkali-aggregate reaction

Alkali-aggregate reactivity occurs in two forms: alkali-silica reaction (ASR) and alkali-carbonate reaction (ACR). It is a type of concrete deterioration that occurs when the active mineral constituents of some aggregates react with the alkali hydroxides in the concrete, as Figure 3.10.



Figure 3.10 Cracks due to Alkali-aggregate reaction, Portland cement association (2005)

Loss of support

Loss of support beneath concrete structures can cause a variety of problems in concrete structures, from cracking and performance problems to structural failure. It usually caused by settling or washout of soils and subbase materials. Loss of support can also occur due to inadequate formwork support or premature removal of forms during construction, as Figure 3.11.



Figure 3.11 Cracks due to Loss of support, Portland cement association (2005)

3.2 Influence of cracks in the initiation period

In this chapter, macro cracks (>0.1mm wide) are discussed, because no information about influence of micro crack (width less than 0.1 mm) was found in the literature. The effect of macro cracks on initiation time is controlled by the cover size, the crack geometry, the concrete properties (mainly the resistivity and the self healing capacity) and the local exposure conditions. The crack geometry and the local exposure conditions are in an uncontrolled way and they may vary extensively. The effects of cracks on chloride and corrosion in concrete structures are not the same in different environment. In sea water submerged cracks without streaming water, the exposure conditions are fairly constant and the measured chloride threshold levels are not as low as for cracked concrete exposed to wetting and drying.

The environment and the corrosion properties may vary extensively in cracks exposed to wetting and drying. As oxygen is abundant, chloride content may be enriched due to the wetting and drying. The chloride threshold levels vary extensively under such conditions, and they are much lower than the levels measured in uncracked concrete. However, if a concrete structure is fully submerged, no reinforcement is exposed to the atmosphere, and thus the chloride threshold can be very high also for cracked concrete. It is probably a result of a lack of oxygen in combination with a high pH and precipitation of calcium carbonates and hydroxides in the crack.

It is very difficult to predict the initiation time in macro cracked reinforced concrete exposed to wetting and drying, because of the consequence of the large variations of environment. However, it is clear that the initiation time for both cracked and uncracked concrete depends on the cover thickness. When compared to uncracked concrete, the initiation time is much lower, Nilsson *et al.* (1997).

3.3 Influence of cracks in the propagation period

Generally, in a given crack pattern, the main parameters controlling the corrosion rate in concrete exposed to atmosphere are the cover thickness and the concrete resistivity. The corrosion propagation rate in a macro crack exposed to air decreases over time because of the clogging of cracks with corrosion products and self healing of cracks. The accumulated corrosion depth in a corrosion pit is shaped similar to a square root function as confirmed in experiments test by Verbetskii *et al.* (1989), Figure 3.12.

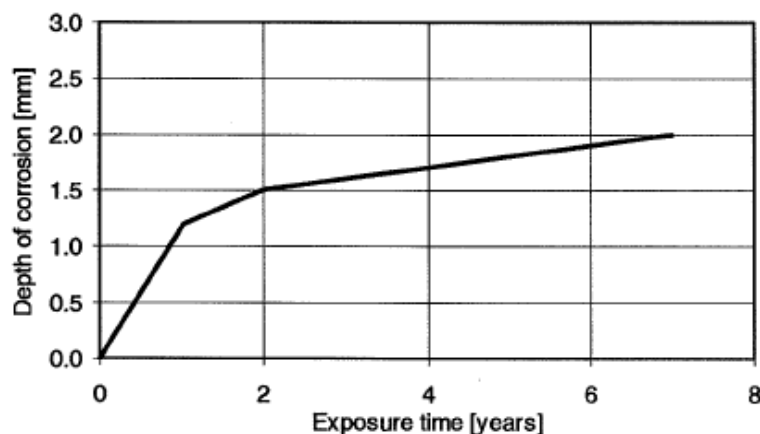


Figure 3.12 Accumulated corrosion depth as a function of time in macro cracked concrete exposed to periodic wetting by 3% NaCl and drying in laboratory exposure, Verbetskii *et al.* (1989)

However, the corrosion process is sometimes accelerated when the microstructure around the corrosion cell is opened due to the spalling of the concrete cover. The macro cell type of corrosion is the most rapid corrosion attack on steel in concrete. It occurs most rapidly in cracks reaching the reinforcement in wet concrete exposed to chloride.

Actually on the short time the propagation rate varies extremely upon wetting and drying. But if the the corrosion process is not leading to any spalling and accelerated corrosion, the general square root tendency illustrated in Figure3.12 seems to be valid in the long term for concrete exposed to air.

In fully submerged concrete, the corrosion rate will be depressed because of the lack of oxygen at the reinforcement, provided that no reinforcement is in metallic connection with reinforcement in concrete exposed to the atmosphere. In this case, the propagation rate will be insignificant in a 100 years service life. An extremely slow type of corrosion can be initiated if the oxygen level is too low to maintain passivity

at very low potential where pitting corrosion can not occur. However, this type of corrosion is so slow that it does not have any practical consequences within a hundred years of service of normal structures, Nilsson *et al.* (1997).

4 Review of existing tests on the influence of cracks on chloride induced corrosion

4.1 Experiment by Francois

4.1.1 Purpose

The aim of the experiment by Francois (1998) was to determine the relationship between cracking in the loaded reinforced concrete and corrosion of embedded steel in a chloride environment. The experiment investigated reinforced concrete beams kept in loading state, in a confined salt fog over 12-year period.

4.1.2 Reinforced concrete sample

Reinforced concrete samples were 3-m long beams, 15 x 28 cm cross section, see Figure 4.1. Type A and B beams had different reinforcement layout but used the same steel with $E_s = 500$ MPa. Type A and B corresponded to a 40mm and 10mm concrete cover respectively.

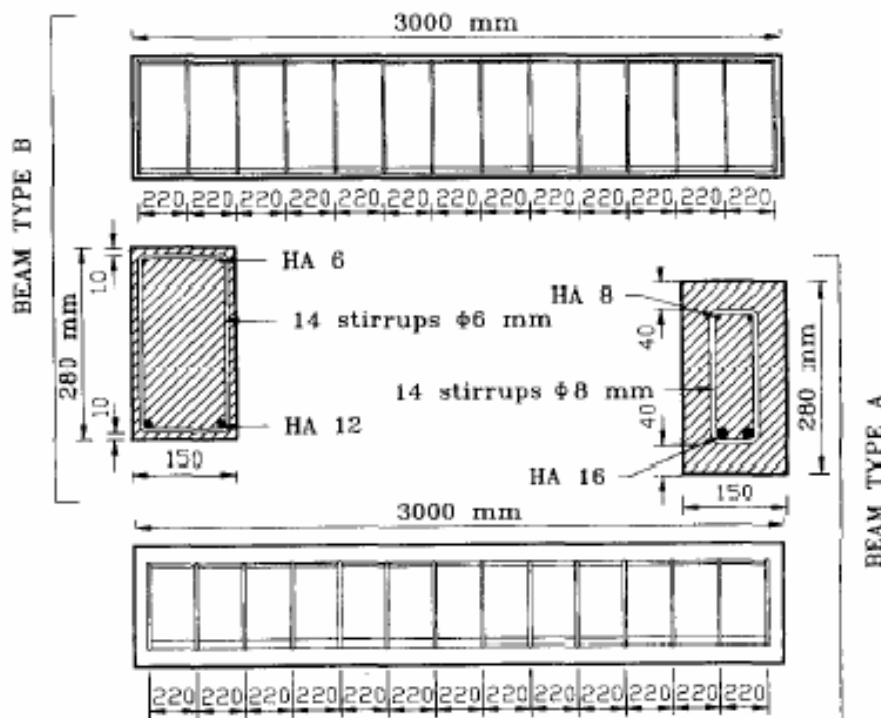


Figure 4.1 Layout of reinforced concrete beams, Francois (1998)

The concrete composition is given in Table 4.1

Table 4.1 Concrete composition, Francois (1998)

Material	Kg/m ³	Slump (cm)	Strength (MPa)
Coarse aggregate	1220	7	45
Sand	820		
Ordinary Portland Cement	400		
Water	200		
W/c	0.5		

4.1.3 Loading and exposure conditions

These beams were loaded by coupling A beam with B beam, kept over a 12-year period, Figure 4.2. In spite of creeping, loading was kept constant. Two loadings were used, the first one was $M_1 = 135$ kNm, the second one was $M_2 = 212$ kNm. Beams A1 and B1 were loaded with the first loading whereas A2 and B2 were loaded with the second one.

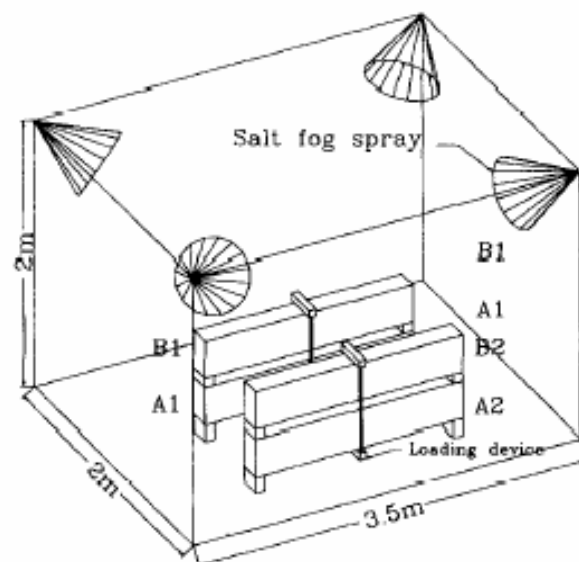


Figure 4.2 Experimental set up and exposure conditions, Francois (1998)

Salt fog (35 g/L of NaCl) was generated by four sprays, using compressed air at 0.1 MPa, located in each upper corner of the confined chamber. Spraying intensity was such that an average 2 cm³/h of solution is at least collected on a 80cm² horizontal

area. The exposure was intermittent spray: 15 days of wetting and 15 days of drying in natural conditions. For each beam, the upper surface corresponded the pouring surface. For all B beams, this surface was the most exposed to salt fog spraying due to that they were located on A beams. Furthermore, four similar beams were stored under the same loadings but in open air as the control group.

4.1.4 Measurements

Destructive tests were carried out to investigate chloride concentration profile, steel corrosion map and steel-concrete interface.

4.1.5 Results

The results indicated that influence of load on the development of the reinforcement corrosion was important than the crack widths. The load applied to reinforced concrete structure influenced the penetration of aggressive agents and thus then the corrosion of reinforcement. The load both increased the chloride penetration and encouraged the development of corrosion in the tensile reinforcement because of the slip between the concrete and the steel. These two effects were clearly visible when the concrete cover was sufficient (A beam) to give good protection for reinforcement. When the concrete cover was small (B beam), the depassivation threshold was quickly reached in every part of the structure, even if the penetration was faster in the tensile zone. The two effects lead to the development of secondary cracks (cracks due to the increase of the volume of rust products) throughout the longitudinal reinforcement.

4.2 Experiment by Mohammed

4.2.1 Purpose

The aim of the experiment by Mohammed *et al.* (2001) was to determine the relationship between crack width and corrosion of steel bar in cracked concrete. The experiment investigated reinforced concrete beams with single and multi cracks. The influence of w/c ratio was investigated also on reinforcement corrosion.

4.2.2 Reinforced concrete sample

Reinforced concrete samples were 10 x 10 x 40 cm for single crack specimens, crack widths were 0.1, 0.3 and 0.7 mm. Multi crack specimens were 15 x 15 x 125 cm with crack width varied from 0.1 to 0.4 mm. These beams were tested over a 13-week period. The concrete composition is illustrated in Table 4.2

Table 4.2 Concrete proportion, Mohammed *et al.* (2001)

Material	Mix 1 (Kg/m ³)	Mix 2 (Kg/m ³)
Coarse aggregate	988	1031
Sand	803	837
Cement	330	236
Water	165	165
Water-reducing agent (ml/m ³)	743	637
Air Entraining (ml/m ³)	13.2	9.5
W/c	0.5	0.7

4.2.3 Loading and exposure conditions

Details of the single crack specimen are shown in Figure 4.3a. After casting, the specimens were cured for 28 days in a closed container at about 20⁰C and 80% RH. A notch was made at the center across the specimen in order to fix the location of the crack at the middle of the specimens. The specimens were cracked with specified crack widths by bending. At the specified cracks, steel sheets were inserted in the cracks to keep them open after removing the load. After cracking, the specimens were

kept in a closed chamber subjected to automatic wetting (3.5% salt water for 24h at 60°C) and drying (60h at 60°C, RH = 80%). Before investigation, the specimens were removed from the chamber and kept in environment of about 20°C, 80% RH. The investigation was last for 13 weeks.

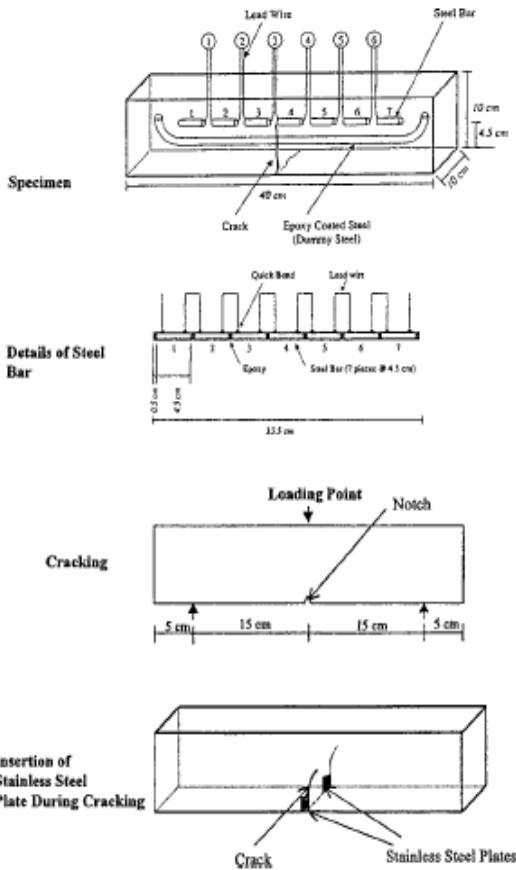


Figure 4.3a Single crack specimens

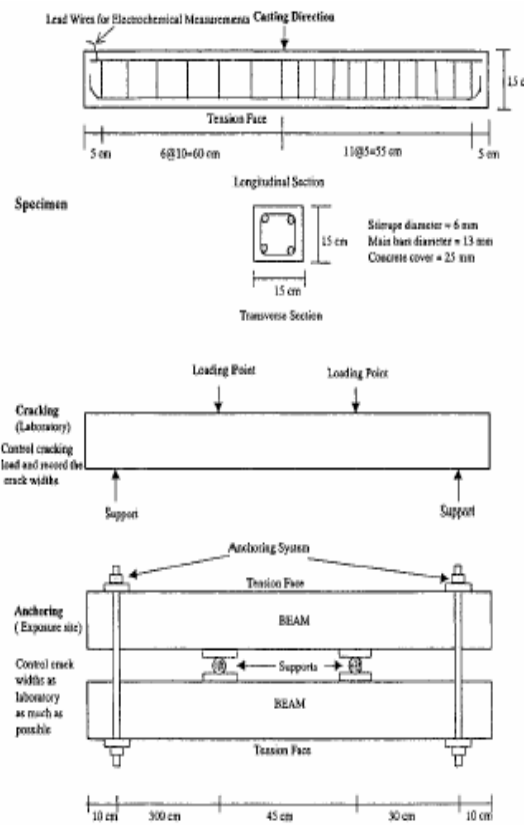


Figure 4.3b Multi crack specimen

Details of the multi crack specimens are shown in Figure 4.3b. After casting, the specimens were cured for 28 days under wet jute bags. The specimens were put at the exposure site under the open sky where they were subjected to 3.5% salt water spray once a week. The crack widths were controlled in the load test as much as possible. For $w/c = 0.5$ and $w/c = 0.7$, the maximum load were 5500 and 4500 kg. The investigation lasted for 16 months.

4.2.4 Measurements

Macro and microcell corrosion were investigated in single crack specimens. Electrochemical investigation was conducted on multi crack specimens. Detail of the measurement is shown in Table 4.3.

Table 4.3 Measurement items, Mohammed et al. (2001)

	Single crack specimen	Multi crack specimen
Measurement	Macrocell and microcell current density	Polarisation resistance

4.2.5 Results

In the experiments, the relation between crack width and corrosion current density were observed at the early age of the exposure. In the beginning of the exposure period (1 – 2 weeks), the larger the crack widths, the higher the corrosion current density. After 4 weeks of exposure, the relation between crack width and corrosion current density changed. It varied moderately or it even decreased.

They concluded that crack widths could be correlated with corrosion in the very beginning of the exposure period only. However the period seems to be small compared to the service life of a structure. The presence of cracks is much more important than its width regarding to corrosion of steel bar in concrete. However, crack widths should be limited for aesthetic reasons. A clear relation between w/c and corrosion rate was observed. Design a concrete mix with a low w/c will increase the compressive strength, therefore limiting the crack widths with the same loads. In the propagation period, the corrosion rate of steel bar was significantly influenced by the surrounding conditions, i.e., oxygen permeability, solution, chloride concentration.

5 Experiments

5.1 Introduction

In order to investigate the influence of minor cracks (width less than 0.2 mm) on the corrosion initiation, three groups of concrete beams were cast. The beams in group A were loaded to cracking, and the load was kept during the test. The beams in group B were loaded to cracking, and thereafter unloaded. The beams in group C were not loaded, and thus uncracked. Group C was considered as a reference group.

Table 5.1 Classification of test specimens

	Group A	Group B	Group C
Beam number	A1, A2, A3	B1, B2	C1, C2
Description	Loaded	Unloaded	Without load

To investigate the influence, half cell potential of these beams were recorded before and during exposure. When the potential dropped under a certain value, it was a signal of corrosion, thus, the initial time to start corrosion was measured. Details of the experiments are described in the following parts.

5.2 Test specimens

For practical reasons, maximum three beams could be cast with the same batch. Beam numbers A1, B1, C1 were in one batch, A2 and B2 were in one, A3 and C2 were in another one. The classification of these test specimens is shown in Table 5.1. The concrete properties are shown in Table 5.2.

Concrete with high w/c ratio (0.77) was designed for these beams. The concrete grade was C20/25. Actual compressive strength of concrete is shown in appendix D. All the beams were 800 mm length and 100 x 150 mm in cross section, see Figure 5.1. Two steel bars with 8 mm in diameter were used for each beam. The free concrete cover to the bottom surface was 20 mm.

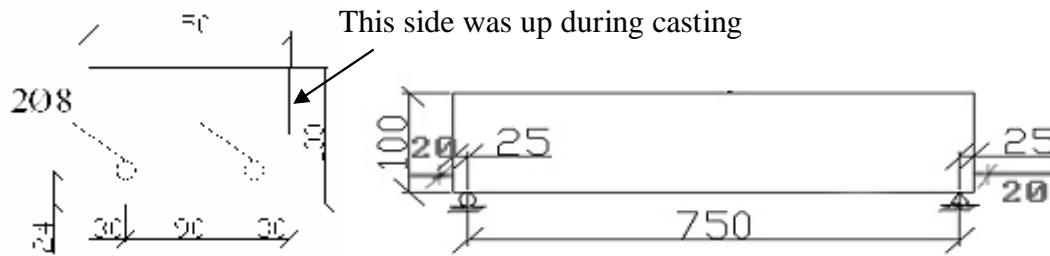


Figure 5.1 Dimensions of test specimens

Table 5.2 Concrete properties

	Design amount for 1m ³	Actual amount for A1, B1, C1	Actual amount for A2, B2	Actual amount for A3, C2
Cement (kg)	252	10.12	10.12	11.3
Gravel (kg)	1263	50.52	50.52	56.8
Macadam, $d_{\max} = 20$ mm (kg)	620	24.8	24.8	27.9
Water (l)	194	7.8	7.8	8.7
Density of fresh concrete (kg/m ³)	2329	2355	2381	2367
Slump (cm)	3 - 5	1.5	3	2.5
W/c ratio	0.77	0.77	0.77	0.77
Compressive strength (MPa)	20	29.92	29.77	28.10

Concrete casting was carried out from the side of the beams where the 10-cm side was parallel to the ground. After casting, all beams were covered by plastic sheets. Formworks were removed for all the beams one day after casting. All beams then were rotated where the 10-cm side was perpendicular to the ground and cured in water for 28 days. When the curing period was finished, the beams in groups A and B were loaded and after unloading the beams in group B, they were exposed to salt water. The beams in group C were exposed to the same salt water as group A and B, but no load was applied on them.

5.3 Loads

The estimation for crack width in the middle of the beams was 0.2 mm, corresponding to a concentrated load of 12 kN in the mid span. Detail of calculation is in appendix C. A lever system was used to create the load of 12 kN, as it was not possible to apply it directly on the beams. In the lever system, a dead load (F) was hung at one end of the lever arm, creating a load (P) in the middle of the beams, see Figures 5.2 and 5.3. The distance between F and P was 2100mm and from P to the other end of the lever arm was 300mm. Therefore, the applied load on the beams was increased 8 times of the dead load. To prevent crushing of the concrete surface, P was applied on a plate with 50 mm width. After curing the beams for 28 days, group A and B were loaded.

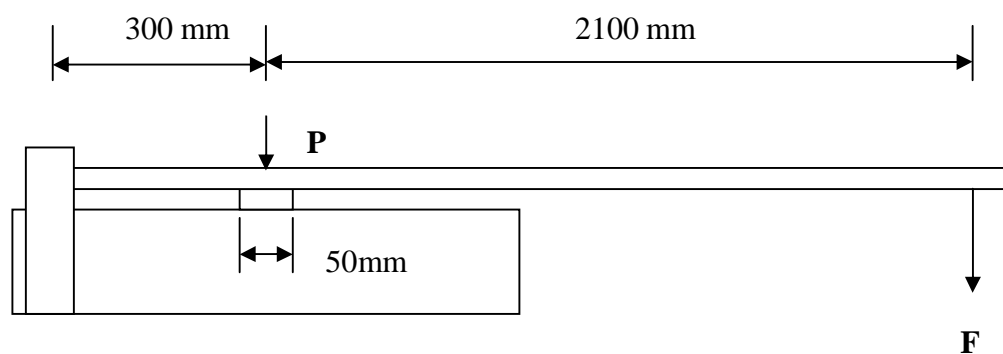


Figure 5.2 Sketch of the lever system



Figure 5.3 Lever system for group A in the laboratory

Load applied on the beams and the supports of the beams are described in Figure 5.4 and 5.5



Figure 5.4 Load applied on the beam



Figure 5.5 Support of the beam

Detail of loads on these beams are listed in Table 5.3.

Table 5.3 Loads on the concrete beams

Beam	A1	A2	A3	B1	B2
F (kN)	1.565	1.544	1.511	1.493	1.493
P (kN)	12.52	12.35	12.09	11.94	11.94

5.4 Crack widths

Crack widths were measured on both sides of the beams. For the test specimens in group A, that were loaded during the test, the crack widths were measured in the beginning stage when load was applied on them. Due to the limited height between the beams and the floor, a plastic sheet with pre-defined widths was used to measure the crack widths. The crack widths of group B were measured after the load was removed. A microscope was used as the beams could be lift up above the ground. A sketch of location of cracks is shown in Figure 5.6. The distance between two cracks was from 5 to 10 cm.

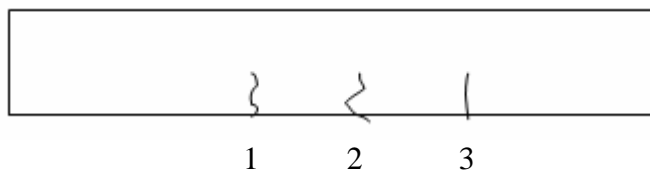


Figure 5.6 Sketch of cracks in concrete beams

For both groups, crack widths and depths were measured on both sides of the beams. The average values of crack widths and depths are shown in Tables 5.4 and 5.5.

Table 5.4 Average crack width and depth for group A

		A1		A2		A3	
Crack		Width	Depth	Width	Depth	Width	Depth
	1st	0.09 mm	38 mm	0.10 mm	32 mm	0.02 mm	75 mm
	2nd	0.10 mm	40 mm	0.08 mm	29 mm	0.05 mm	45 mm
	3rd	0.08 mm	72 mm	-	-	0.02 mm	43 mm
	Average	0.09 mm	50 mm	0.09 mm	31 mm	0.03 mm	60 mm

Table 5.5 Average crack width and depth for group B

		B1		B2	
Crack		Width	Depth	Width	Depth
	1 st	0.03 mm	12 mm	0.03 mm	20 mm
	2 nd	0.02 mm	45 mm	0.02 mm	34 mm
	3 rd	0.02 mm	28 mm	-	-
	Average	0.027 mm	43 mm	0.025 mm	27 mm

5.5 Exposure conditions

After loading to create crack in group A, the specimens were exposed to salt water. For group B, they were exposed to salt water after cracking and removal of the load. No load was applied on group C. The age of the beams was about one month at that time. All three groups were in the same exposure condition with NaCl = 10% in the solution, corresponding to 6.7% chloride concentration. This was higher than the chloride concentration in big oceans (2%). The reason to choose high concentration of chloride was to accelerate the corrosion in the experiments.

The temperature and relative humidity in the laboratory were around 23⁰C and 30% respectively. To keep these beams in contact with the solution all the time, a piece of textile was attached in the bottom of each beam. The contacting length along the beam was 20 cm. The other part of the textile was put into a box containing the solution as can be seen in Figure 5.7. All cracks of the beams and half of the beam were exposed to the solution, Figure 5.8.



Figure 5.7 Exposure conditions of concrete beam for three group A, B and C

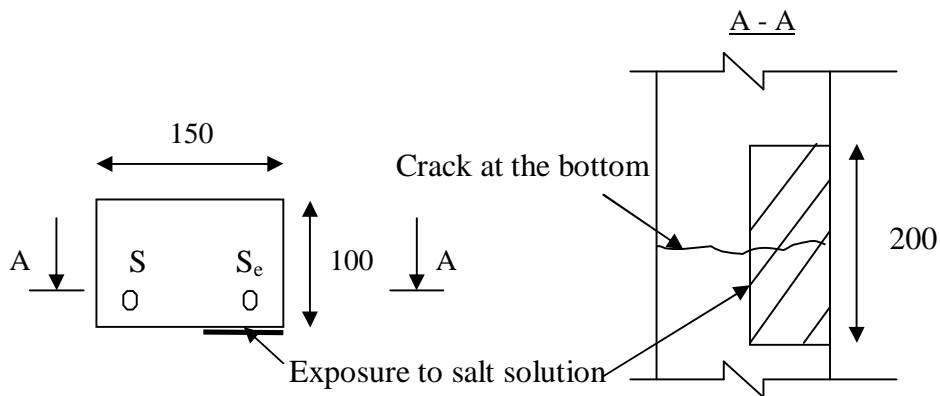


Figure 5.8 Half of the beam in contact with the solution. S_e : steel bar directly exposed to salt solution, S : steel bar indirectly exposed to salt solution.

To prevent the evaporation, a cover was used for the box. Everyday, the box was filled with salt water, compensating for the vapour amount. However the concentration of chloride was increased as the evaporation could not be totally prevented.

5.6 Measurements

5.6.1 Half cell potential measurements

The measurements were carried out on the sides of the beams as the distance from the reinforcement to the concrete surface is small compared to the top of the beams. ASTM C 876-91 requires the minimum spacing between two measured points to

provide at least a 100 mV difference between readings. However, it can be applied only for a large area, thus, distance between 2 points was randomly chosen to be 120 mm, Figure 5.9. The measurements were done on one side of the beam, where it was exposed to the solution.

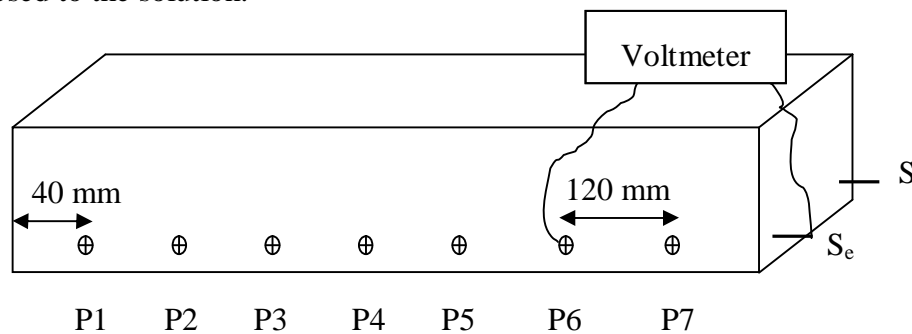


Figure 5.9 Chosen points for measuring in concrete beams

In general, the procedure for measurement was in accordance with ASTM C 876-91, some minor adjustment was done for practical reason. The procedure was as follow:

- Sprinkle water on the concrete beams three times with an interval of 5 minutes to pre-wet the concrete surface. This work was to decrease the electrical resistance of the concrete.
- Measure the potential in each point of the concrete beam using silver/silver chloride half cell circuitry, as Figure 5.9. A wet small textile was needed to create good connection between the electrode and concrete surface.
- When the voltage readings between two measurements at the same point were stable (no variation than ± 0.02 V), they were recorded.



Figure 5.10 Half cell potential measurement

5.6.2 Corrosion rate measurement

Count and guard electrode was used to measure the corrosion rate of reinforcement, resistivity of concrete and half cell potential of reinforcement, Tang (2002). However, the results for corrosion rate measured by this tool were not stable due to the exposure conditions were too dry. The results for resistivity were according to the wet conditions of the concrete beams. The electrical potential results were similar to the ones measured by silver/silver chloride electrode. This was to confirm the accuracy of silver/silver chloride electrode. The half cell potential results measured by both methods are shown in appendix E.

5.6.3 Destructive measurement

In order to investigate the corrosion rate of reinforcement, the test samples were broken. Figure 5.11 shows the surface of a concrete beam, including cracks and rust products. Only bending cracks were visible, i.e. no specimen showed any signs of cracks due to corrosion. After breaking, it was observed that there was only pitting corrosion in the middle of the reinforcement bars. An example of pitting corrosion on the reinforcement bars is in Figure 5.12



Figure 5.11 Crack and rust products on the surface of a specimen

Cleaning procedures of reinforcement were in accordance with ASTM G1-03. Mechanical cleaning was applied on the reinforcement bars. Each steel bar was cleaned manually five times and finally by a machine. The interval time between each cleaning cycle was 5 minutes. The weight of the steel bar was recorded before and after each cycle.

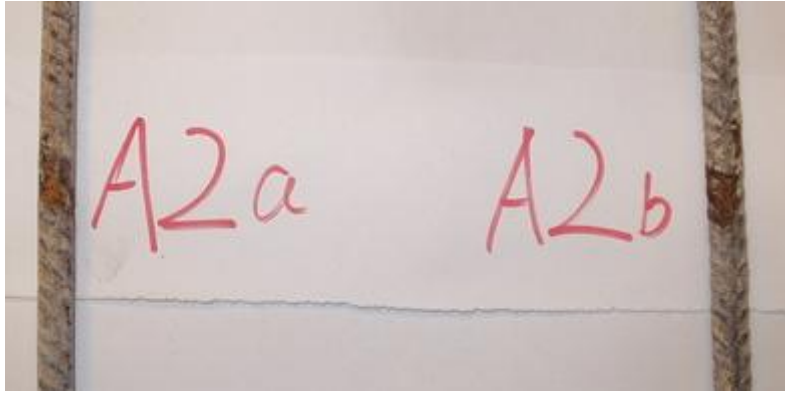


Figure 5.12 Pitting corrosion in the middle of steel bars. A2a: steel bar directly exposed to salt solution, A2b: steel bar indirectly exposed to salt solution.

The corrosion rate was calculated as follows:

$$\text{Corrosion rate} = (K \times W) / (A \times T \times D)$$

Where:

- K: a constant, depending on the units. If the corrosion rate is calculated mm/year, $K = 8.76 \times 10^4$
- W: mass loss in g
- A: Area of steel bar in cm^2 . In case of pitting corrosion, a string was used to measure the length along the reinforcement bar and the length around the perimeter of the bar to calculate the corrosion area (A_p). In case of uniform corrosion, corrosion area (A_u) was calculated from the weight of the steel bar after cleaning (W_a), $A_u = 8 W_a / (D R)$, R was radius of the steel bar, $R = 0.4$ cm.
- T: Time of exposure in hour, calculating from time from corrosion take places until time when breaking the specimens
- D: Density of steel bar in g/cm^3 , $D = 7.86 \text{ g/cm}^3$.

5.7 Results

5.7.1 Half cell potential results

Group A

The electrical potential results for the beams with cracks and loads are shown in Figures 5.13, 5.14, 5.15. These figures show the electrical potential in the middle point (P4) and two points at the ends of the beam (P1, P7).

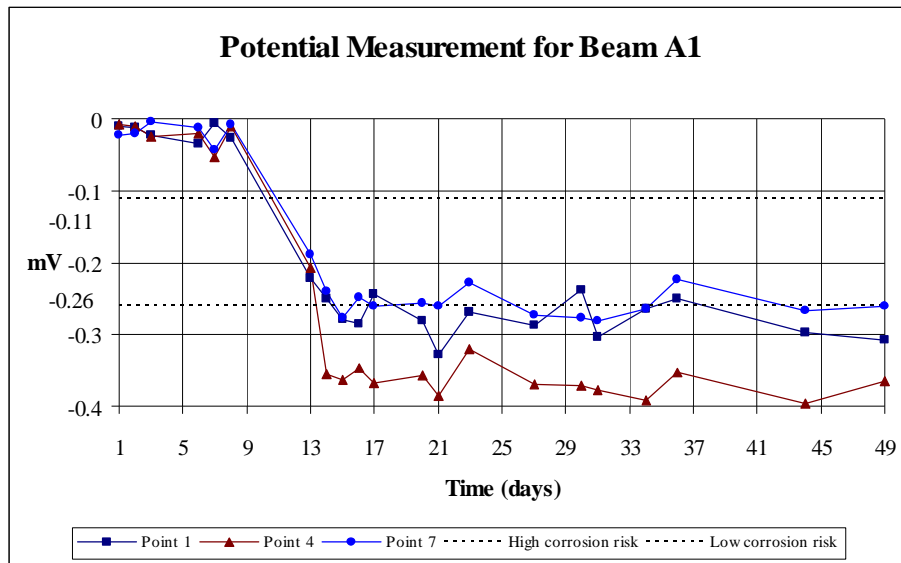


Figure 5.13 Half cell potential results for beam A1

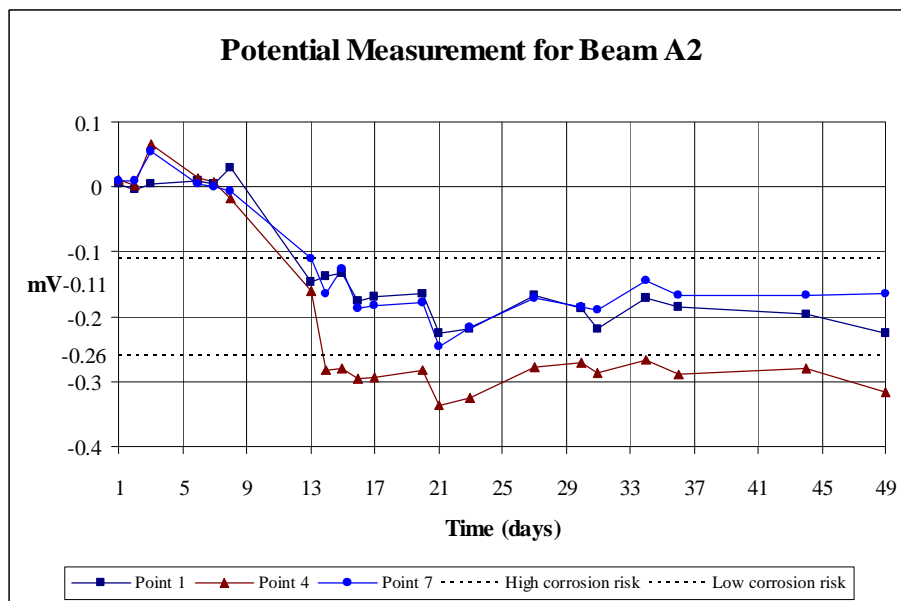


Figure 5.14 Half cell potential results for beam A2

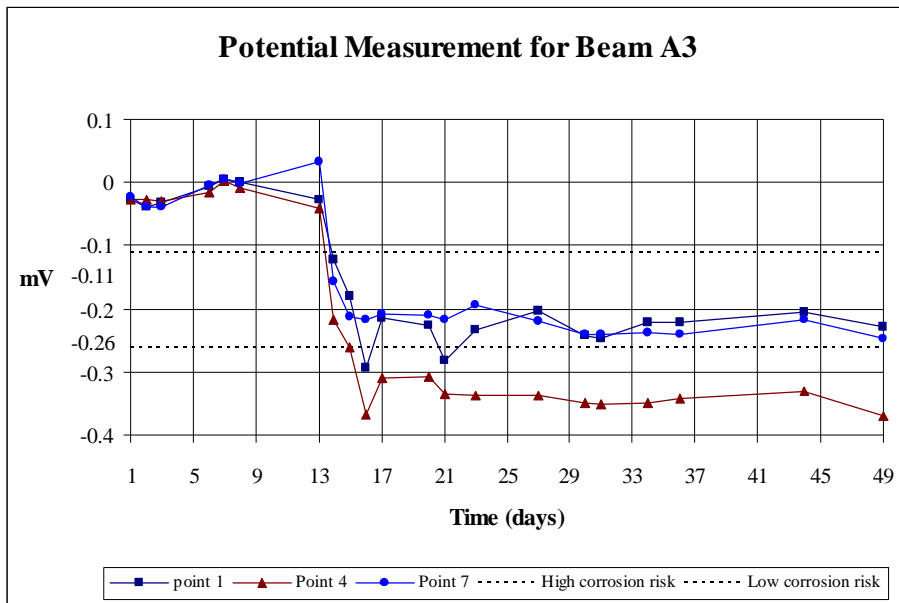


Figure 5.15 Half cell potential results for beam A3

Before and after corrosion happened, the potential varied moderately. According to ASTM C867, the reinforcement is in high risk of corrosion when the electric potential is below - 0.26 mV. Thus, when the electrical potential dropped suddenly (less than - 0.26 mV), it could be considered as a sign of corrosion of the reinforcement in group A. The approximate time for corrosion to start in each point are listed in Table 5.6.

Table 5.6 Approximate time for corrosion to start (days)

Point number	P1	P4	P7
Beam A1	14 - 15	13 - 14	14 - 15
Beam A2	-	13 - 14	-
Beam A3	-	15	-

According to the Table 5.6, corrosion happened in the middle of the beam A1 first as it was exposed to salt water. Thereafter, both ends of the beam started to corrode after one to two days. From the measurements, it was uncertain to know whether both ends of the beams A2 and A3 were corroding or not as the electrical potentials were above -0.26 mV. Most likely, the measuring points were too close to each other, thus, corrosion in the middle effected the measurements in point P1 and P7.

Group B

The electrical potential results for cracked and unloaded beams are shown in Figures 5.16, 5.17. These figures show the potential in the middle point (P4) and two points at the ends of the beam (P1, P7).

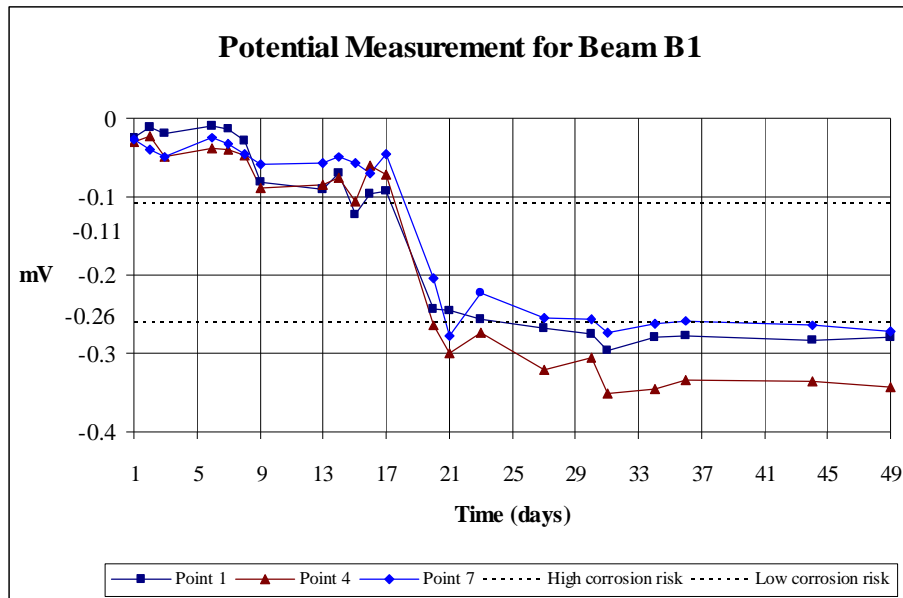


Figure 5.16 Half cell potential results for beam B1

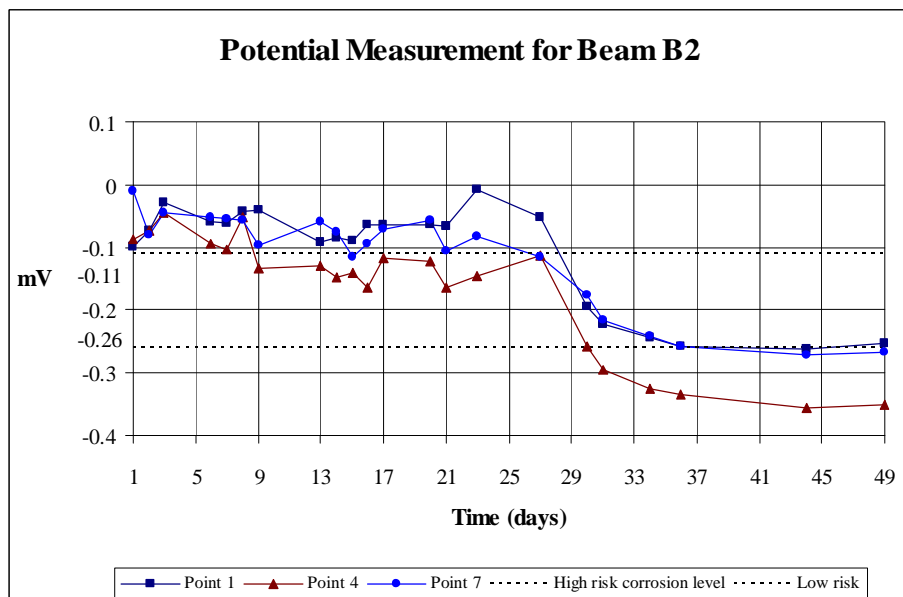


Figure 5.17 Half cell potential results for beam B2

Similarly to group A, when the electrical potential drop less than -0.26 mV, it could be considered as a sign of corrosion in the reinforcement in group B. The approximate time for corrosion to start in each point are in Table 5.7.

Table 5.7 Approximate time for corrosion to start (days)

Point number	P1	P4	P7
Beam B1	27	20	27
Beam B2	44	30	44

According to Table 5.7, corrosion happened in middle of the beam B1 and B2 after 20 and 30 days. The same comments as for group A is valid concerning the measurements at the end of the beams.

Group C

The electrical potential results for the middle point P4 and the two points at the ends of the beams P1, P7 are shown in Figures 5.18, 5.19. Corrosion had not started yet for 49 days since they had been exposed to salt solution.

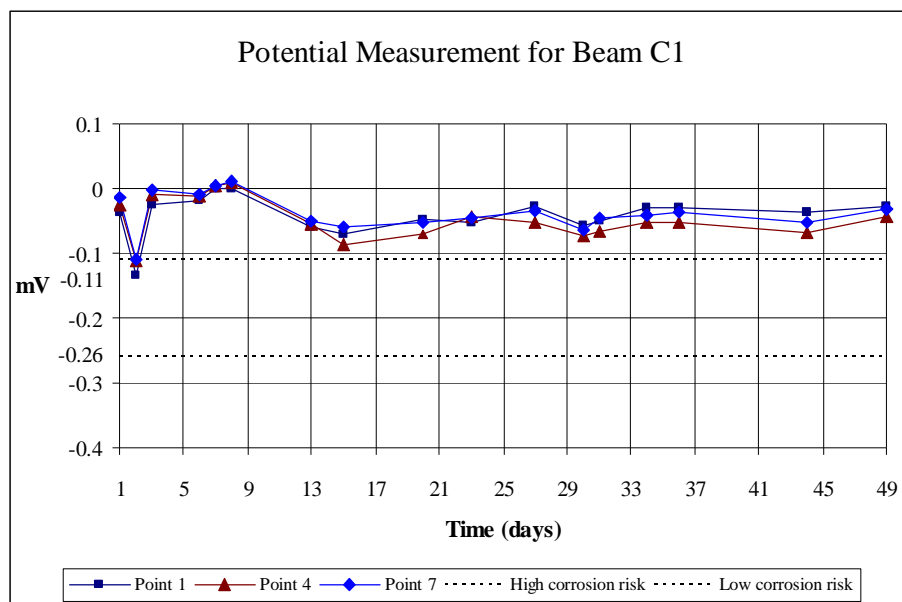


Figure 5.18 Half cell potential results for beam C1

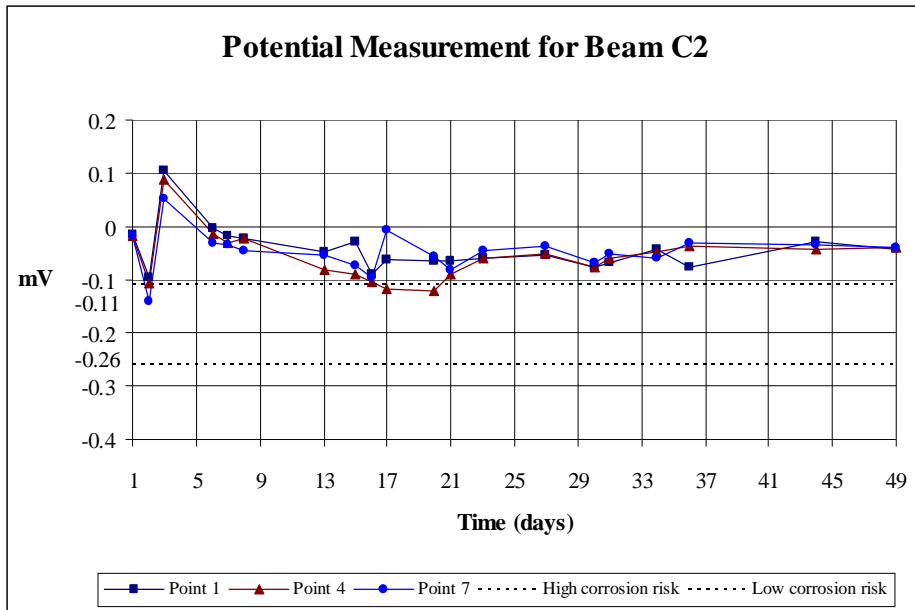


Figure 5.19 Half cell potential results for beam C2

Comparison of all beams

To investigate the initial corrosion time, the potentials of all beams at the end (P1) and in the middle (P4) are illustrated in Figure 5.20 and 5.21.

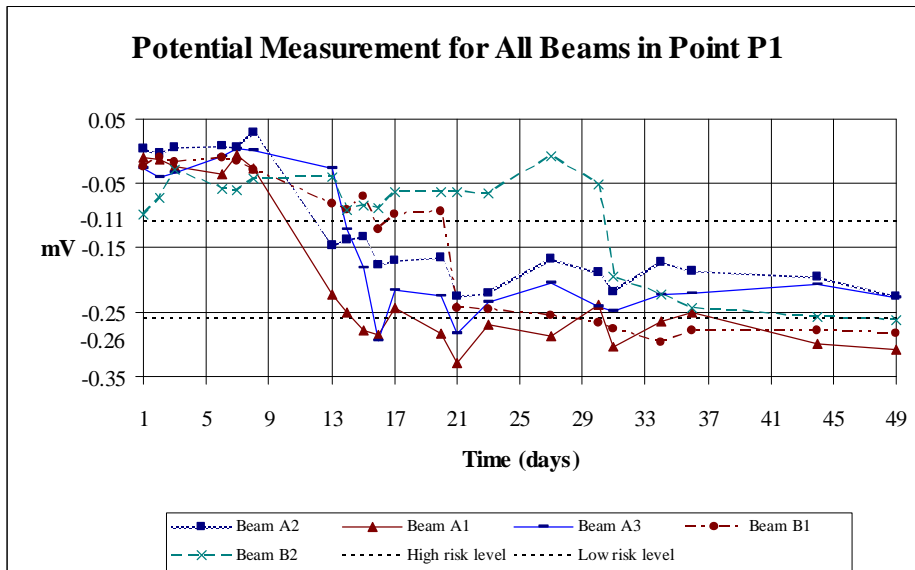


Figure 5.20 Half cell potential results for point P1

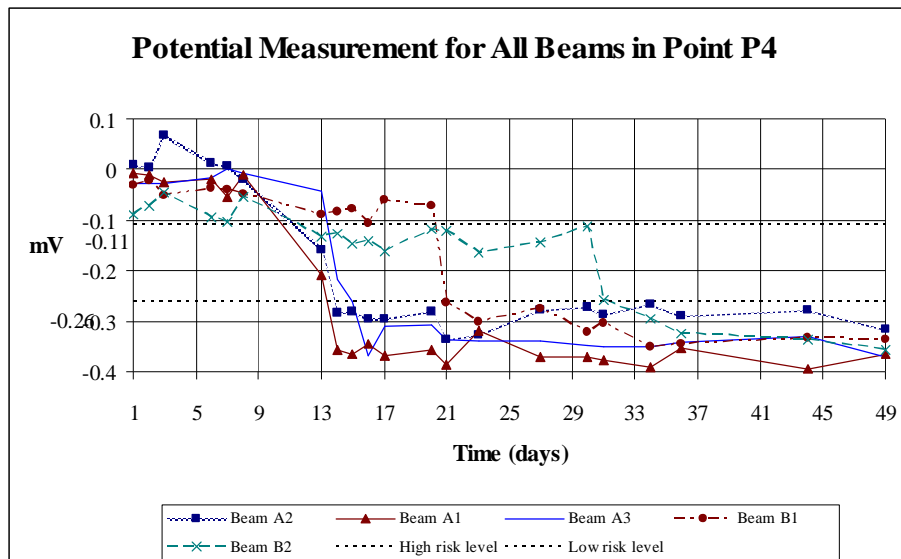


Figure 5.21 Half cell potential results for point P4

In summary, the starting date of corrosion in group A and B is illustrated in Table 5.8.

Table 5.8 Approximate time for corrosion to start in group A and B (days)

	A1	A2	A3	B1	B2	C1	C2
P1	14 -15	-	-	27	44	-	-
P4	13 -14	13 - 14	15	20	30	-	-

There was no corrosion in the uncracked beams C1 and C2 since they had been exposed to salt solution for nearly two months while the cracked specimens started to corrode after only 2 – 4 weeks. Thus, from these results, the presence of cracks had a negative effect on the initiation time.

From the Table 5.8 above, it is clear that the beams in group A started to corrode earlier than in group B. Thus, the fact that the cracks in group B were smaller due to removal of the load, influenced in a positive way. The experiment confirm the results of Francois (1998), that load play an important role to corrosion. Group A with loads during the test started corroding before group B which had no load.

The initiation corrosion time between beam B1 and B2 was also different. One possible reason for this difference could be the variation of the amount of the absorbed solution. During the exposure time, it was noted that the daily amount of solution put in the box for B1 was more than for B2. Remaining oil from the

formwork in the surface of the concrete beams could be one reason for different amount of absorbed solution.

5.7.2 Destructive results

The weight loss corresponding to cleaning cycles is put in appendix F. Pitting and uniform corrosion rate are listed in Table 5.9.

Table 5.9 Pitting and uniform corrosion rate

	A1		A2		A3		B1		B2	
	S _e	S	S _e	S						
Before exposure (W _b) (g)	323.67	320.44	321.31	324.23	321.19	325.58	320.37	324.94	324.66	321.21
After exposure (W _a) (g)	322.81	319.49	320.44	323.15	320.27	324.52	319.92	324.17	323.91	320.54
W=W _b -W _a (g)	0.86	0.95	0.87	1.08	0.92	1.06	0.45	0.77	0.75	0.67
K	87600									
T (h)	1682				1646		1526		1286	
D (g/cm ³)	7.86									
A ₁ (cm ²)	2.5	2	1	1	0.5	1	1	1	3.5	1.5
A ₂ (cm ²)	102.67	101.62	101.92	102.78	101.87	103.22	101.76	103.11	103.02	101.95
Pitting Corrosion rate (mm/year)	2.279	3.147	5.765	7.156	12.459	7.177	3.287	5.624	1.857	3.871
Uniform Corrosion rate (mm/year)	0.055	0.062	0.057	0.070	0.061	0.070	0.032	0.055	0.063	0.057

(S_e and S were the reinforcement bars directly and indirectly exposed to salt solution respectively)

The corrosion rate depends on the weight loss (W) and the area of corrosion A_p or A_u . The weight loss was measured by high accuracy in comparison with the pitting corrosion area, which was manually measured. Therefore, the value of weight loss seems more reliable than the area of pitting corrosion. As a result, the uniform corrosion rate is more reliable than the pitting one. The uniform corrosion rate therefore calculated even though it was known that it was pitting corrosion.

6 Conclusions and suggestions for further research

All five cracked beams already started to corrode in the first month, the earliest one (A1 and A2) started after two weeks, and the last one (B2) started after one month. Two beams without cracks (C1, C2) had not started to corrode since they had been exposed to salt solution for nearly two months. The relation between the average crack width and initial corrosion time of the cracked beams are illustrated in Figure 6.1.

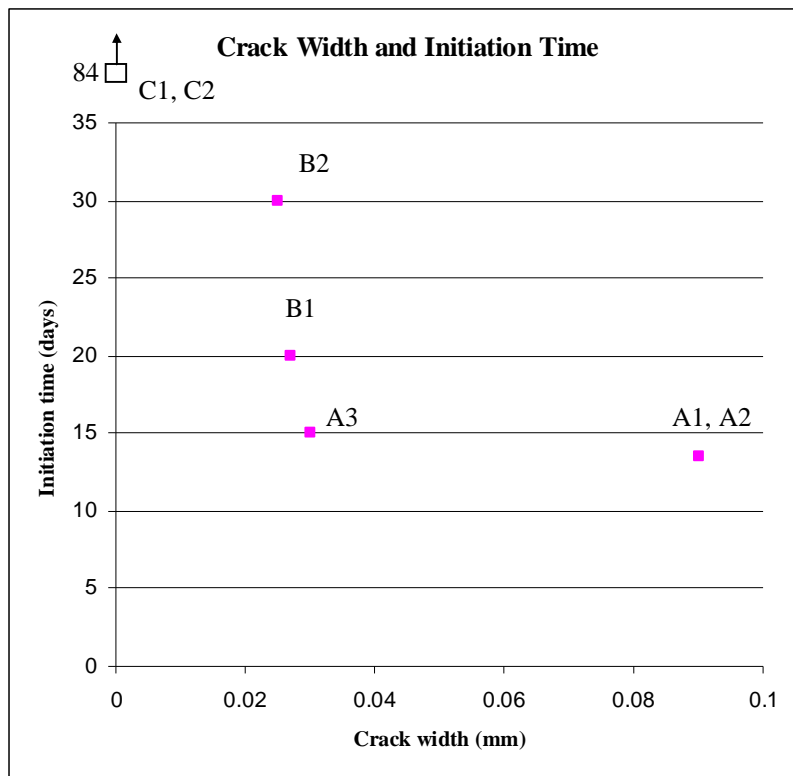


Figure 6.1 Average crack width and initiation corrosion in the middle of the beams

From these results, it is clear that cracks influence the corrosion initiation time. The larger the crack width, the earlier the initiation of corrosion. When the crack width increased from 0.025 to 0.027 mm, the initiation time reduced from 30 to 20 days whereas the initiation time decreased from 20 to 15 days when the crack width increased from 0.027 to 0.03 mm. When the crack width increased from 0.03 to 0.09 mm, the initiation time decreased to 13 – 14 days. It was obvious that the relation between crack width and initiation time was not linear.

In the experiments, beam B1 started to corrode earlier than B2 although the crack width was not so different. Beam B1 absorbed more solution than B2, i.e. the

permeability of B1 was higher than B2. This could be a reason to explain the difference initiation between two beams.

Figure 6.2 illustrates the relation between crack width and the uniform corrosion rate of a steel bar in the beam that has largest corrosion rate.

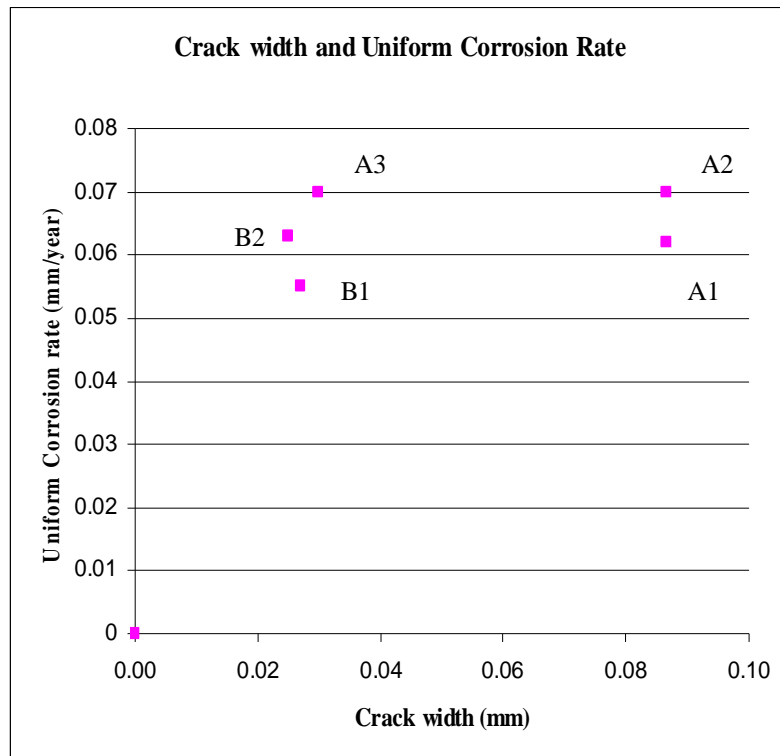


Figure 6.2 Crack width and uniform corrosion rate

It was clear that the relation between crack width and uniform corrosion rate was also not linear. The results in Figure 6.1, 6.2 showed that the larger the crack width, the shorter the initiation time and the higher the uniform corrosion rate. It could be concluded that the simple experiment in the thesis was able to investigate the influence of crack on corrosion.

Due to the limited time for the thesis, the corrosion was accelerated in a short time. As a result, the test specimens were cast with low concrete grade. In addition, they were exposed to high concentration of chloride. In fact, real structures usually have better grade of concrete and an adequate cover thickness. The maximum chloride concentration in seawater is less than the salt solution in the experiment above. Thus, to investigate the influence of crack on the corrosion, some recommendations are suggested as follows:

- Increase and vary the thickness of the concrete cover. It is estimated that the thicker cover, the longer the initiation time.

- Decrease the w/c of concrete to increase the compressive strength. When concrete has higher compressive strength the permeability of concrete will decrease, therefore, the higher the compressive strength, the longer the initiation time.
- Reduce the concentration of the chloride solution. How the concentration of chloride influence on the initial corrosion period is questionable. It is recommended that the concentration of chloride to be varied in new experiments to clarify this matter.
- Vary the width of the cracks and vary the number of cracks in contact with chloride solution. Crack width is related to load. It is suggested that calculations are made to estimate the crack width and that the load in the laboratory is adjusted to achieve the designed crack width. By varying the exposure length of the beam, the number of cracks in contact with chloride can also be varied.
- To increase the accuracy of the measurement for the weight loss of steel bars, a cleaning machine should be used for the bar before casting and after destructive test.
- Finally, investigate the test specimens with the same crack width in different exposure conditions such as dry and wet cycle.

When more data is available, it will be possible to develop a model to predict the initiation and propagation period. Ideally, the model will estimate the time for uncracked and cracked specimens to start corroding. It will predict the time when the threshold value of chloride is reached.

7 References

ASTM (1991), Standard Test Method for Half-Cell Potentials of Uncoated Reinforcing Steel in Concrete, American Society for testing and Materials Standards, Designation: C 876-91, 1991.

ASTM (2003), Standard Practice for Preparing, Cleaning, and Evaluating Corrosion Test Specimens, American Society for testing and Materials Standards, Designation: G1-03, 2003.

Benjamin, S. E and Sykes, J. M (1990): Corrosion of Reinforcement in Concrete. Elsevier Applied Science, London, 1990, 59 pp.

Broomfield, J.P. (1997): Corrosion of Steel in Concrete, Understanding, Investigation and Repair. E&FN Spon, 1997, 240 pp.

DuraCrete (1999): Models for Environmental Actions on Concrete Structures. The European Union – Brite EuRam III, 1999, 273 pp.

Engström B.(2004): Structural Concrete, Chalmers University of Technology, 2004, 384 pp

Francois, R and Arliguie, G (1998): Influence of Service Cracking on Reinforcement Steel Corrosion. Journal of Material in Civil Engineering, 1998, pp. 14-20.

Goodbrake, C.J. & Young, J.F & Berger, R.L (1979): Reaction of hydraulic calcium silicates with carbon dioxide and water, Journal of American Ceramic Society, Vol 62, No 9-10, 1979, 488 pp.

Isgor O.B., Razaqpur A.G. (2004): Finite element modeling of coupled heat transfer, moisture transport and carbonation process in concrete structures, Cement and Concrete Composites, Volume 26, Issue 1, January 2004, pp. 57-73.

Maslehuddin, M. (1996): Effect of Temperature on Pore Solution Chemistry and Reinforcement Corrosion in Contaminated Concrete. The Royal Society of Chemistry, Thomas Graham House, Science Park, Cambridge CB4 4WF, 1996, pp. 68-75.

Millard S.G, Ghassemi M.H, Bugey J, Jafar, M.I (1990): Assessing the Electrical Resistivity of Concrete Structures for Corrosion Durability Studies, Corrosion of Reinforcement in Concrete (Eds.: Page, Treadaway, Bamforth), Elsevier, London, 1990, pp. 303-313.

Nilsson L-O., Poulsen E., Sandberg P., Sorensen H.E., Klinghoffer O.(1996): Hetek, Report No.53, 1996, 151pp

Nilsson L-O., Sandverg P., E.Poulsen E., Tang L., Andersen A.& Fredriksen J,M. (1997): Hetek, Report No.83, 1997, 160pp

Nilsson, L-O. (1980): Hygroscopic moisture in concrete - drying, measurements and related material properties, Building Materials, Lund Institute of Technology, TVBM-1003, Lund, 1980.

Nilsson, L-O. & Peterson, O. (1983): Alkali-silica reactions in Scania, Sweden - A moisture problem causing popouts in concrete floors, Lund Institute of Technology, Report TVBM-3014, Lund, 1983.

Nordtest, (1989): Concrete, repairing materials and protective coating: UDC 691.32:658.588, NT Bulid 357, Tekniikantie 12, FIN-20150 Espoo, Finland, 1989, pp 1-2

Ohata, T. (1991): Corrosion of Reinforcement Steel in Concrete Exposed to Sea Air. CANMET/ACI, Montreal, Canada. 1991. pp 459-477.

Otsuki, N., Miyazato, S., Diola N., Suzuki H.: Influences of Bending crack and Water-Cement Ratio on Chloride-Induced Corrosion of Main Reinforcing Bars and Stirrups. ACI Material Journal/ July-August 2000, pp. 454-464

Parrott, L J (1996): Water absorption, Chloride Ingress and Reinforcement Corrosion in Cover Concrete: Some Effects of Cement and Curing. The Royal Society of Chemistry, Thomas Graham House, Science Park, Cambridge CB4 4WF, 1996, pp. 152-154.

Pettersson, K (1992): Corrosion Threshold Value and Corrosion Rate in Reinforced Concrete in Concrete. Swedish Cement and Concrete Research Institute, S-100 44 Stockholm, 1992, pp. 30-31.

Portland cement association (2005): Portland cement association, http://www.cement.org/tech/faq_cracking.asp [10-2005]

Rodriguez, J. (1994): On Site Corrosion Rate Measurements in Concrete Structures Using a Device Developed under Eureka Project EU-401. Proc. of International conference on Concrete Across Borders Vol.1, Odense, Denmark, Jun 1994, pp 171-185.

Schiessl, P and Raupach, M. (1990): Corrosion of Reinforcement in Concrete. Elsevier Applied Science, London, 1990, 59 pp.

Steffens A., Dinkler D., Ahrens H. (2002): Modeling Carbonation for Corrosion Risk Prediction of Concrete Structures, Cement and Concrete Research, Volume 32, Issue 6, June 2002, pp. 935-941.

Tang L. (2002): Mapping Corrosion of Steel in Reinforced Concrete Structures. SP Swedish National Testing and Research Institute Building Technology Sp report 2002:32, 62 pp

Tuutti, K. (1982): Corrosion of Steel in Concrete. Swedish Cement and Concrete Research Institute, Stockholm, Report No.CBI Research 4:82, 1982, 468 pp.

APPENDIX A: Cement types in Parrott's research

Name	Cement content	Cement content
D54		CEMI
U1		CEMI
U2	85% U1 + 15% Limestone	CEMII/A-L
U3	75% U1 + 25% Limestone	CEMII/B-L
U4		CEMI
U5	85% U4 + 15% Limestone	CEMII/A-L
U6	75% U4 + 25% Limestone	CEMII/B-L
U7	50% U4 + 50% GGBS	CEMIII/A
U8	25% U4 + 75% GGBS	CEMIII/B
U9	75% U4 + 25% GGBS	CEMIII/B-S
F1		CEMI
F2		CEMI
F3		CEMI
F4	75% F2 + 25% Limestone	CEMII/B-L
F5	79% F1 + 19% Limestone	CEMII/A-L
F6	80% F3 + 5% FPA + 5% GGBS + 10% LS	CEMII/A-M
F7		CEMIII/C

APPENDIX B: Record of potential measurement

A1	Value								Note
	1	2	3	4	5	6	7	V	
February 1	-0.011	-0.01	-0.01	-0.009	-0.013	-0.016	-0.022		Measure on top of the beam
February 2	-0.013	-0.012	-0.01	-0.011	-0.014	-0.013	-0.02		
February 3	-0.023	-0.01	-0.009	-0.024	-0.024	-0.003	-0.005		
February 6	-0.035	-0.044	-0.039	-0.02	-0.05	-0.029	-0.012		
February 7	-0.006	-0.019	-0.006	-0.054	-0.073	-0.085	-0.044		
February 8	-0.026	-0.068	-0.018	-0.01	-0.045	-0.04	-0.009		
February 13	-0.222	-0.193	-0.279	-0.208	-0.247	-0.179	-0.189		Measure in side of the beam
February 14	-0.25	-0.272	-0.333	-0.355	-0.361	-0.304	-0.241		
February 15	-0.278	-0.19	-0.244	-0.364	-0.293	-0.253	-0.276		
February 16	-0.285	-0.28	-0.343	-0.346	-0.347	-0.306	-0.248	0.244	
February 17	-0.244	-0.303	-0.35	-0.367	-0.375	-0.317	-0.26	0.175	
February 20	-0.282	-0.295	-0.343	-0.357	-0.364	-0.308	-0.257	0.278	
February 21	-0.329	-0.341	-0.393	-0.386	-0.383	-0.334	-0.261	0.23	
February 23	-0.269	-0.257	-0.302	-0.319	-0.328	-0.282	-0.228	0.254	
February 27	-0.288	-0.319	-0.353	-0.37	-0.381	-0.336	-0.272	0.283	
March 2	-0.238	-0.316	-0.253	-0.372	-0.383	-0.337	-0.277	0.28	
March 3	-0.303	-0.324	-0.361	-0.378	-0.387	-0.338	-0.28	0.244	
March 6	-0.265	-0.322	-0.369	-0.391	-0.393	-0.347	-0.264	0.091	
March 8	-0.251	-0.29	-0.33	-0.353	-0.356	-0.308	-0.224	0.107	
March 16	-0.298	-0.349	-0.375	-0.395	-0.395	-0.348	-0.267	0.039	
March 21	-0.308	-0.303	-0.333	-0.365	-0.369	-0.314	-0.26	-0.041	

V: electrical potential measured between two steel bars.

A2	Value								Note
	1	2	3	4	5	6	7	V	
February 1	0.004	0.006	0.01	0.011	0.012	0.012	0.01		Measure on top of the beam
February 2	-0.003	0.002	0.005	0.003	0.001	0.009	0.009		
February 3	0.006	0.008	0.013	0.067	0.05	0.065	0.055		
February 6	0.009	0.016	0.014	0.013	-0.011	0.008	0.005		
February 7	0.005	0.008	0.012	0.008	-0.009	-0.002	0.001		
February 8	0.03	0.025	0.005	-0.018	-0.043	-0.01	-0.006		
February 13	-0.147	-0.098	-0.154	-0.16	-0.175	-0.167	-0.11		Measure in side of the beam
February 14	-0.138	-0.15	-0.236	-0.283	-0.286	-0.25	-0.164		
February 15	-0.132	-0.122	-0.235	-0.281	-0.284	-0.177	-0.127	0.104	
February 16	-0.177	-0.171	-0.248	-0.296	-0.291	-0.239	-0.188	-0.104	
February 17	-0.169	-0.16	-0.24	-0.294	-0.286	-0.236	-0.183	-0.091	
February 20	-0.164	-0.165	-0.243	-0.282	-0.273	-0.237	-0.178	-0.06	
February 21	-0.226	-0.224	-0.316	-0.337	-0.325	-0.304	-0.247	-0.088	
February 23	-0.22	-0.233	-0.302	-0.326	-0.319	-0.278	-0.217	-0.053	
February 27	-0.167	-0.159	-0.243	-0.278	-0.272	-0.24	-0.172	-0.107	
March 2	-0.188	-0.163	-0.233	-0.272	-0.267	-0.24	-0.186	-0.106	
March 3	-0.218	-0.194	-0.258	-0.288	-0.285	-0.25	-0.19	-0.111	
March 6	-0.172	-0.175	-0.232	-0.266	-0.256	-0.238	-0.145	-0.127	
March 8	-0.185	-0.18	-0.256	-0.289	-0.291	-0.25	-0.167	-0.07	
March 16	-0.196	-0.179	-0.239	-0.279	-0.273	-0.23	-0.166	-0.078	
March 21	-0.226	-0.218	-0.281	-0.316	-0.316	-0.284	-0.165	-0.078	

V: electrical potential measured between two steel bars.

A3	Value								Note
	1	2	3	4	5	6	7	V	
February 1	-0.027	-0.029	-0.028	-0.027	-0.015	-0.028	-0.022		Measure on top of the beam
February 2	-0.04	-0.041	-0.044	-0.028	-0.026	-0.026	-0.039		
February 3	-0.033	-0.039	-0.028	-0.029	-0.027	-0.033	-0.038		
February 6	-0.007	-0.007	-0.01	-0.016	-0.007	-0.01	-0.004		
February 7	0.004	0.013	0.004	0.002	-0.001	0.013	0.005		
February 8	0.001	-0.001	-0.003	-0.008	-0.011	-0.014	-0.002		
February 13	-0.027	-0.026	-0.018	-0.041	-0.04	-0.01	0.033		Measure on side of the beam
February 14	-0.122	-0.135	-0.19	-0.216	-0.234	-0.193	-0.157		
February 15	-0.181	-0.208	-0.252	-0.26	-0.29	-0.248	-0.212		
February 16	-0.294	-0.304	-0.355	-0.368	-0.381	-0.367	-0.216	0.048	
February 17	-0.215	-0.218	-0.282	-0.31	-0.299	-0.263	-0.207	0.055	
February 20	-0.226	-0.235	-0.273	-0.308	-0.302	-0.268	-0.211	0.048	
February 21	-0.282	-0.238	-0.307	-0.336	-0.321	-0.29	-0.217	0.064	
February 23	-0.234	-0.24	-0.31	-0.338	-0.333	-0.299	-0.193	0.036	
February 27	-0.204	-0.232	-0.308	-0.338	-0.352	-0.298	-0.22	0.022	
March 2	-0.242	-0.25	-0.31	-0.348	-0.338	-0.295	-0.24	0.038	
March 3	-0.248	-0.252	-0.319	-0.352	-0.341	-0.306	-0.241	0.026	
March 6	-0.222	-0.244	-0.326	-0.35	-0.345	-0.308	-0.239	0.018	
March 8	-0.221	-0.24	-0.315	-0.341	-0.336	-0.297	-0.24	0.021	
March 16	-0.206	-0.23	-0.307	-0.33	-0.323	-0.275	-0.216	0.006	
March 21	-0.228	-0.253	-0.327	-0.37	-0.362	-0.322	-0.248	-0.036	

V: electrical potential measured between two steel bars.

B1	Value								Note
	1	2	3	4	5	6	7	V	
February 1	-0.025	-0.026	-0.025	-0.031	-0.057	-0.062	-0.027		Measure on top of the beam
February 2	-0.011	-0.01	-0.012	-0.023	-0.051	-0.055	-0.04		
February 3	-0.018	-0.019	-0.033	-0.05	-0.061	-0.063	-0.049		
February 6	-0.01	-0.007	-0.03	-0.038	-0.051	-0.049	-0.025		
February 7	-0.014	-0.009	-0.018	-0.039	-0.076	-0.06	-0.032		
February 8	-0.029	-0.024	-0.03	-0.048	-0.068	-0.061	-0.045		
February 9	-0.082	-0.034	-0.066	-0.089	-0.086	-0.079	-0.058		Measure on side of the beam
February 13	-0.09	-0.07	-0.091	-0.084	-0.098	-0.074	-0.056		
February 14	-0.07	-0.05	-0.07	-0.076	-0.078	-0.051	-0.049		
February 15	-0.122	-0.09	-0.097	-0.105	-0.087	-0.077	-0.057		
February 16	-0.097	-0.042	-0.07	-0.061	-0.066	-0.074	-0.07	0.081	
February 17	-0.093	-0.063	-0.079	-0.072	-0.058	-0.043	-0.045	0.024	
February 20	-0.244	-0.218	-0.252	-0.264	-0.256	-0.235	-0.203	0.203	
February 21	-0.245	-0.226	-0.282	-0.3	-0.286	-0.253	-0.278	0.185	
February 23	-0.256	-0.228	-0.268	-0.274	-0.297	-0.27	-0.223	0.206	
February 27	-0.267	-0.255	-0.287	-0.321	-0.313	-0.289	-0.254	0.231	
March 2	-0.275	-0.244	-0.297	-0.305	-0.318	-0.301	-0.256	0.233	
March 3	-0.297	-0.282	-0.23	-0.351	-0.338	-0.314	-0.274	0.24	
March 6	-0.279	-0.272	-0.323	-0.345	-0.332	-0.311	-0.263	0.26	
March 8	-0.278	-0.272	-0.321	-0.334	-0.329	-0.310	-0.259	0.261	
March 16	-0.283	-0.275	-0.32	-0.335	0.326	-0.311	-0.265	0.266	
March 21	-0.28	-0.277	-0.328	-0.344	-0.338	-0.313	-0.272	0.274	

V: electrical potential measured between two steel bars.

B2	Value								Note
	1	2	3	4	5	6	7	V	
February 1	-0.099	-0.087	-0.082	-0.088	-0.064	-0.044	-0.01		Measure on top of the beam
February 2	-0.072	-0.068	-0.08	-0.072	-0.072	-0.069	-0.081		
February 3	-0.029	-0.032	-0.049	-0.045	-0.054	-0.04	-0.045		
February 6	-0.059	-0.06	-0.085	-0.095	-0.089	-0.059	-0.052		
February 7	-0.062	-0.07	-0.102	-0.103	-0.089	-0.067	-0.054		
February 8	-0.042	-0.056	-0.083	-0.053	-0.056	-0.048	-0.057		
February 9	-0.041	-0.046	-0.128	-0.133	-0.174	-0.052	-0.097		Measure on side of the beam
February 13	-0.091	-0.013	-0.17	-0.128	-0.18	-0.127	-0.059		
February 14	-0.084	-0.103	-0.14	-0.148	-0.142	-0.09	-0.076		
February 15	-0.089	-0.135	-0.159	-0.141	-0.157	-0.122	-0.116		
February 16	-0.063	-0.087	-0.163	-0.163	-0.145	-0.099	-0.095	0.095	
February 17	-0.063	-0.093	-0.127	-0.117	-0.123	-0.094	-0.07	-0.15	
February 20	-0.064	-0.084	-0.117	-0.121	-0.119	-0.074	-0.056	-0.16	
February 21	-0.066	-0.115	-0.168	-0.165	-0.167	-0.116	-0.105	-0.077	
February 23	-0.008	-0.075	-0.145	-0.145	-0.143	-0.07	-0.082	-0.14	
February 27	-0.052	-0.079	-0.116	-0.112	-0.112	-0.078	-0.115	-0.153	
March 2	-0.195	-0.218	-0.255	-0.257	-0.248	-0.196	-0.175	-0.003	
March 3	-0.223	-0.25	-0.294	-0.294	-0.293	-0.242	-0.216	0.002	
March 6	-0.244	-0.284	-0.324	-0.325	-0.323	-0.27	-0.241	0.033	
March 8	-0.257	-0.233	-0.284	-0.335	-0.284	-0.235	-0.257	0.052	
March 16	-0.261	-0.314	-0.351	-0.355	-0.351	-0.293	-0.271	0.061	
March 21	-0.253	-0.305	-0.352	-0.352	-0.35	-0.29	-0.266	0.053	

V: electrical potential measured between two steel bars.

C1	Value								V	Note
	1	2	3	4	5	6	7			
February 1	-0.036	-0.036	-0.031	-0.024	-0.021	-0.021	-0.013		Measure on top of the beam	
February 2	-0.134	-0.139	-0.118	-0.111	-0.108	-0.112	-0.109			
February 3	-0.025	-0.028	-0.015	-0.009	-0.004	-0.004	-0.003			
February 6	-0.018	-0.026	-0.012	-0.011	-0.008	-0.009	-0.01			
February 7	0.001	0.002	0.001	0.005	0.006	0.008	0.005			
February 8	0.001	0.001	0.011	0.01	0.011	0.008	0.012			
February 13	-0.059	-0.048	-0.062	-0.054	-0.066	-0.035	-0.049		Measure on side of the beam	
February 15	-0.07	-0.049	-0.058	-0.086	-0.052	-0.061	-0.058			
February 20	-0.048	-0.035	-0.079	-0.07	-0.05	-0.063	-0.052	0.09		
February 23	-0.053	-0.034	-0.074	-0.043	-0.032	-0.035	-0.045	0.013		
February 27	-0.027	-0.023	-0.056	-0.053	-0.046	-0.029	-0.035	0.009		
March 2	-0.056	-0.053	-0.076	-0.073	-0.058	-0.055	-0.064	0.012		
March 3	-0.049	-0.042	-0.065	-0.065	-0.048	-0.045	-0.045	0.01		
March 6	-0.03	-0.037	-0.054	-0.052	-0.048	-0.029	-0.042	0.008		
March 8	-0.029	-0.034	-0.054	-0.053	-0.045	-0.033	-0.037	0.012		
March 16	-0.036	-0.032	-0.071	-0.069	-0.053	-0.039	-0.052	0.008		
March 21	-0.027	-0.024	-0.043	-0.043	-0.044	-0.026	-0.031	0.008		

V: electrical potential measured between two steel bars.

C2	Value								Note
	1	2	3	4	5	6	7	V	
February 1	-0.015	-0.015	-0.02	-0.019	-0.011	-0.019	-0.017		Measure on top of the beam
February 2	-0.096	-0.098	-0.113	-0.108	-0.101	-0.116	-0.14		
February 3	0.104	0.11	0.089	0.087	0.097	0.075	0.053		
February 6	-0.005	-0.015	-0.021	-0.016	-0.01	-0.024	-0.031		
February 7	-0.018	-0.003	-0.037	-0.031	-0.033	-0.027	-0.034		
February 8	-0.023	-0.023	-0.021	-0.022	-0.01	-0.026	-0.045		
February 13	-0.047	-0.058	-0.066	-0.081	-0.079	-0.075	-0.053		Measure on side of the beam
February 15	-0.03	-0.057	-0.088	-0.089	-0.076	-0.086	-0.074		
February 16	-0.089	-0.087	-0.103	-0.103	-0.105	-0.099	-0.095		
February 17	-0.063	-0.093	-0.127	-0.117	-0.123	-0.094	-0.007		
February 20	-0.064	-0.084	-0.117	-0.121	-0.119	-0.074	-0.056		
February 21	-0.066	-0.082	-0.09	-0.089	-0.088	-0.09	-0.083	-0.01	
February 23	-0.06	-0.071	-0.058	-0.06	-0.065	-0.056	-0.046	-0.01	
February 27	-0.055	-0.052	-0.048	-0.052	-0.049	-0.048	-0.037	0	
March 2	-0.077	-0.082	-0.075	-0.076	-0.077	-0.076	-0.067	-0.003	
March 3	-0.069	-0.065	-0.061	-0.059	-0.063	-0.065	-0.051	-0.006	
March 6	-0.044	-0.05	-0.047	-0.047	-0.047	-0.063	-0.059	0.002	
March 8	-0.077	-0.063	-0.056	-0.037	-0.044	-0.039	-0.031	-0.004	
March 16	-0.03	-0.046	-0.043	-0.043	-0.045	-0.039	-0.035	-0.001	
March 21	-0.043	-0.046	-0.041	-0.04	-0.04	-0.041	-0.039	-0.003	

V: electrical potential measured between two steel bars.

APPENDIX C: Design calculation for load and crack widths

Input Data

F_{ctm} (28)	Concrete C20/25	0.0015	kN/mm ²
E_{cm}		29	kN/mm ²
E_s		200	kN/mm ²
F_{yk}		0.5	kN/mm ²
c	Cover	24	mm
h	Height	100	mm
b	Width	150	mm
Φ_{steel}	Steel Diameter	8	mm ²
P	Load	12	kN
L	Length of the beam	800	mm

Calculation

As	$2 \cdot (3,14 \Phi_{\text{steel}}^2/4)$	100.48	mm ²
k	$0,6 + 0,4/(0,001h)^{0,25}$	1.311	
F _{ct} (28 day)	$k \cdot F_{ctm} (28)$	0.002	kN/mm ²
β _{cc} (t)	$\exp[0,25*(1-(28/7)^{0,5})]$	0.991	mm
β _E (t)	$\beta_{cc}(t)^{0,5}$	0.995	mm
F _{ct} (7 day)	$\beta_{cc}(t) \cdot F_{ct} (28 \text{ day})$	0.0019	kN/mm ²
E _{cm} (7day)	$\beta_E(t) E_{cm}$	28.86	kN/mm ²
ds	h - c	76	mm
α	$E_s / E_{cm} (7 \text{ day})$	6.929	
x	$[-\alpha \cdot A_s + (\alpha^2 \cdot A_s^2 + 2 \cdot b \cdot d \cdot \alpha \cdot A_s)^{0,5}] / b$	22.32	mm
e	ds - x	53.68	mm
A _{II}	$b \cdot x + \alpha \cdot A_s$	4044.64	mm ²
I _I	$b \cdot h^3/12$	12500000	mm ⁴
I _{II}	$b \cdot x^3/12 + b \cdot x \cdot (x/2)^2 + \alpha \cdot A_s \cdot e^2$	2562226	mm ⁴
M	$P \cdot (L-100)/4 + 22 \cdot 10^{-9} \cdot b \cdot h \cdot L^2/8$	2126.40	kN.mm
σ _c	$M \cdot e/I_{II}$	0.045	kN/mm ²
σ _s	$\alpha \cdot \sigma_c$	0.309	kN/mm ²
M_{cr}	$F_{ct} (7 \text{ day}) \cdot I_I \cdot 2/h$	487.12	kN.mm
σ _{sr}	$\alpha \cdot \sigma_c \cdot M_{cr}/M$	0.071	kN/mm ²
ε _{sm}	$\sigma_s/E_s \cdot (1-(\sigma_{sr}/\sigma_s)^2)$	0.00146	
A _{ef}	$2,5 \cdot b \cdot c$	9000	mm ²
ρ _r	A_s/A_{ef}	0.011	
ε _{rm}	$50+0,25 \cdot \Phi_{\text{steel}} \cdot 0,5 \cdot 0,8/\rho_r$	121.66	
w_k	$1,3 \cdot \epsilon_{rm} \cdot \epsilon_{sm}$	0.231	mm

APPENDIX D: Actual compressive strength

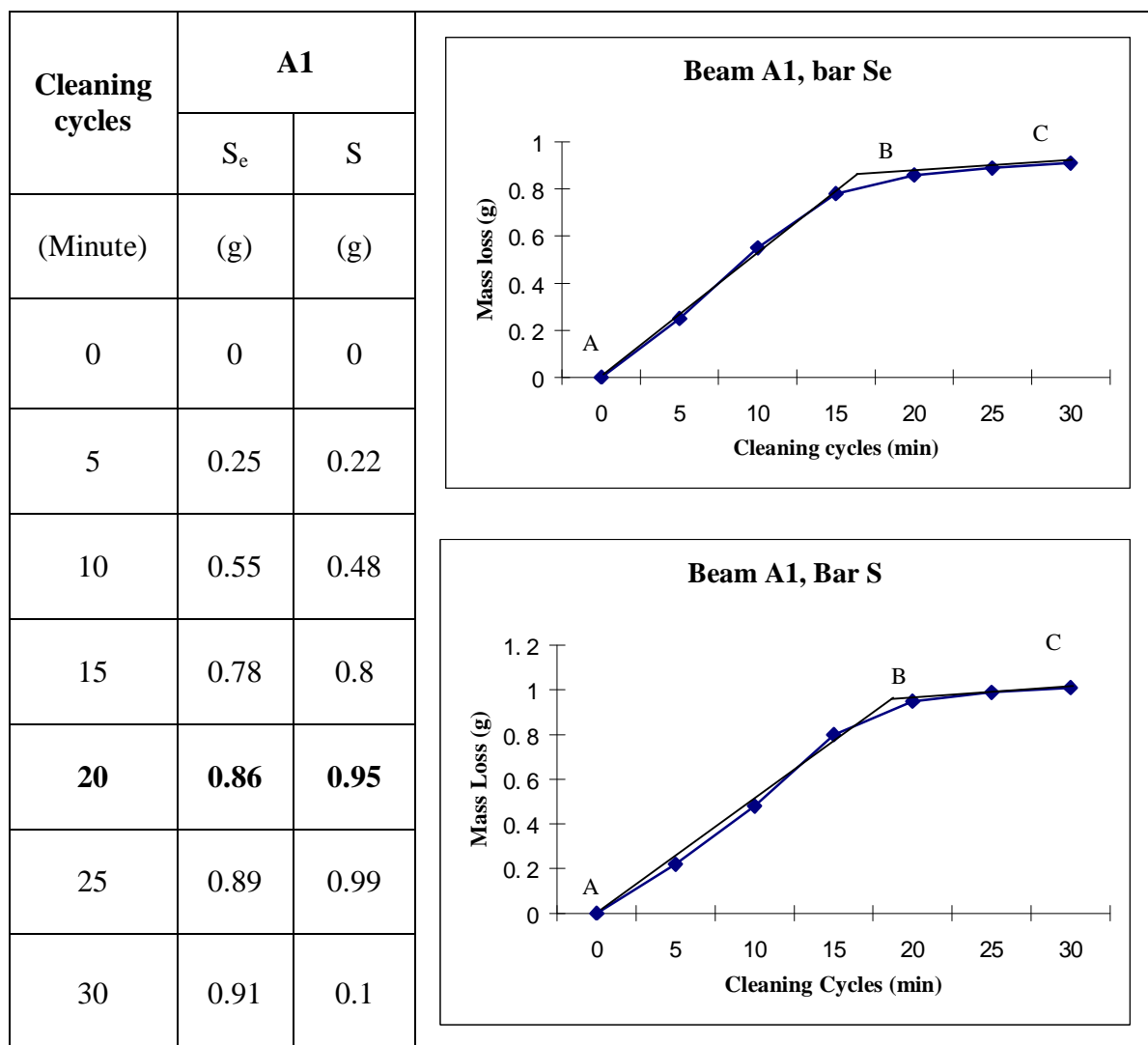
Beam	Casting date	Testing date	Size		Load (kN)	Compressive Strength (MPa)	Average compressive strength (MPa)				
			(cm)	(cm)							
A1, B1, C1	Dec 23, 05	Feb 2, 06	10	10.2	310	30.4	29.92				
			10	10.1	303	30.0					
			10	10.18	294	28.9					
			10	10.1	307	30.4					
A2, B2			Dec 23, 05	Feb 2, 06	9.95	10.2	299	29.5	29.77		
					10	10.1	300	29.7			
					10	10.5	304	29.0			
					10	10.05	311	30.9			
A3, C3					Dec 23, 05	Feb 2, 06	10	10.2	289	28.3	28.10
							10.1	9.6	283	29.2	
							10.02	10.25	278	27.1	
							9.9	10.1	278	27.8	

APPENDIX E: comparison between count/guard and silver/silver chloride electrode in electrical potential measurement

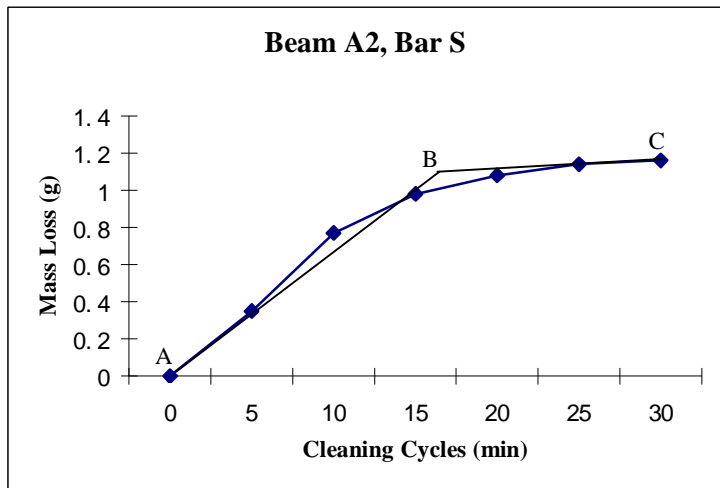
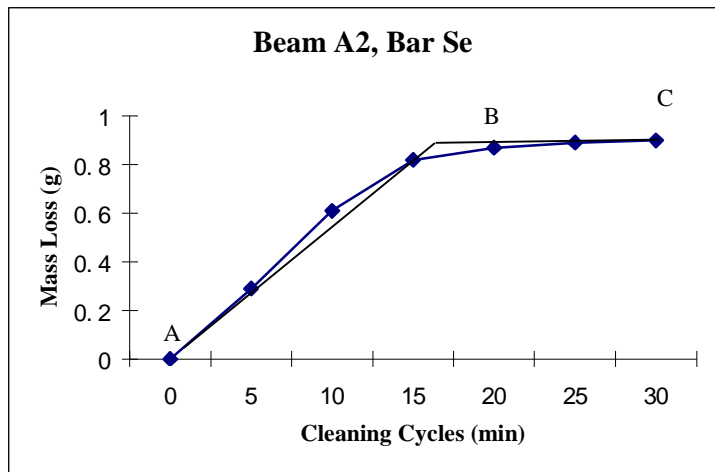
		Point 1	Point 2	Point 3	Point 4	Point 5	Point 6
		(mV)	(mV)	(mV)	(mV)	(mV)	(mV)
A1	Count and guard electrode	-0.359	-0.4	-0.35	-0.361	-0.401	-0.304
	Silver/silver chloride electrode	-0.322	-0.368	-0.335	-0.34	-0.358	-0.287
A2	Count and guard electrode	-0.255	-0.346	-0.28	-0.36	-0.423	-0.385
	Silver/silver chloride electrode	-0.201	-0.28	-0.248	-0.328	-0.357	-0.332
A3	Count and guard electrode	-0.272	-0.388	-0.23	-0.31	-0.372	-0.19
	Silver/silver chloride electrode	-0.252	-0.348	-0.299	-0.265	-0.332	-0.212
B1	Count and guard electrode	-0.322	-0.354	-0.316	-0.036	-0.055	-0.023
	Silver/silver chloride electrode	-0.256	-0.308	-0.289	-0.038	-0.049	-0.03
B2	Count and guard electrode	-0.343	-0.395	-0.34	-0.265	-0.326	-0.242
	Silver/silver chloride electrode	-0.269	-0.308	-0.281	-0.201	-0.275	-0.221
C1	Count and guard electrode	-0.035	-0.069	-0.053	-0.013	-0.021	-0.029
	Silver/silver chloride electrode	-0.049	-0.068	-0.058	-0.02	-0.038	-0.035
C2	Count and guard electrode	-0.075	-0.075	-0.081	-0.039	-0.021	-0.06
	Silver/silver chloride electrode	-0.048	-0.051	-0.051	-0.033	-0.048	-0.039

APPENDIX F: Relation between mass loss of reinforcement bars and cleaning cycles

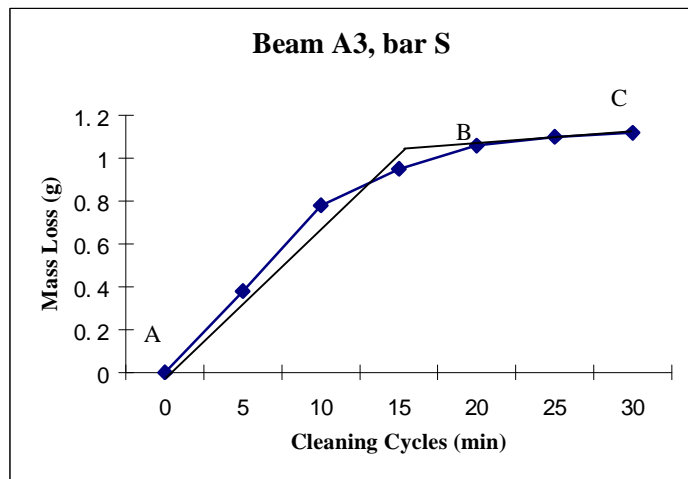
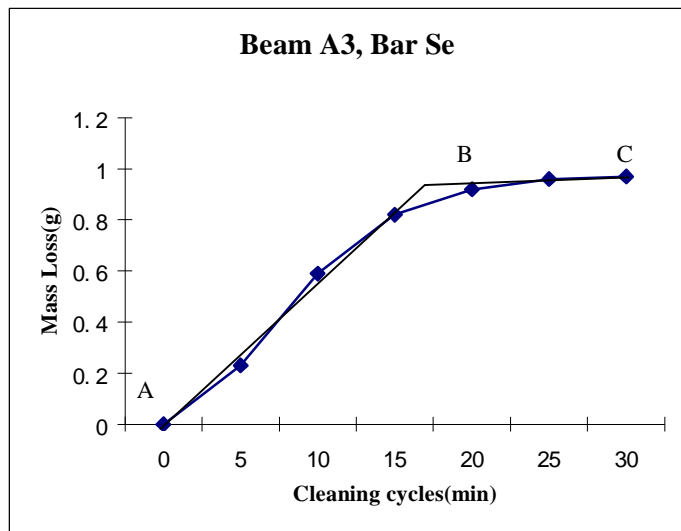
The mechanical method for cleaning after testing was accordance with ASTM G1-03. The mass loss was a graph function of equal cleaning cycles. Two lines were obtained: AB and BC. The later corresponded to corrosion of reinforcement bar after removal of corrosion products. The mass loss due to corrosion corresponded approximately to point B in the graph or the high light numbers in the table. To minimise the uncertainty associated with corrosion of the bars, the line BC was chosen to provide the lowest slope (near to horizontal).

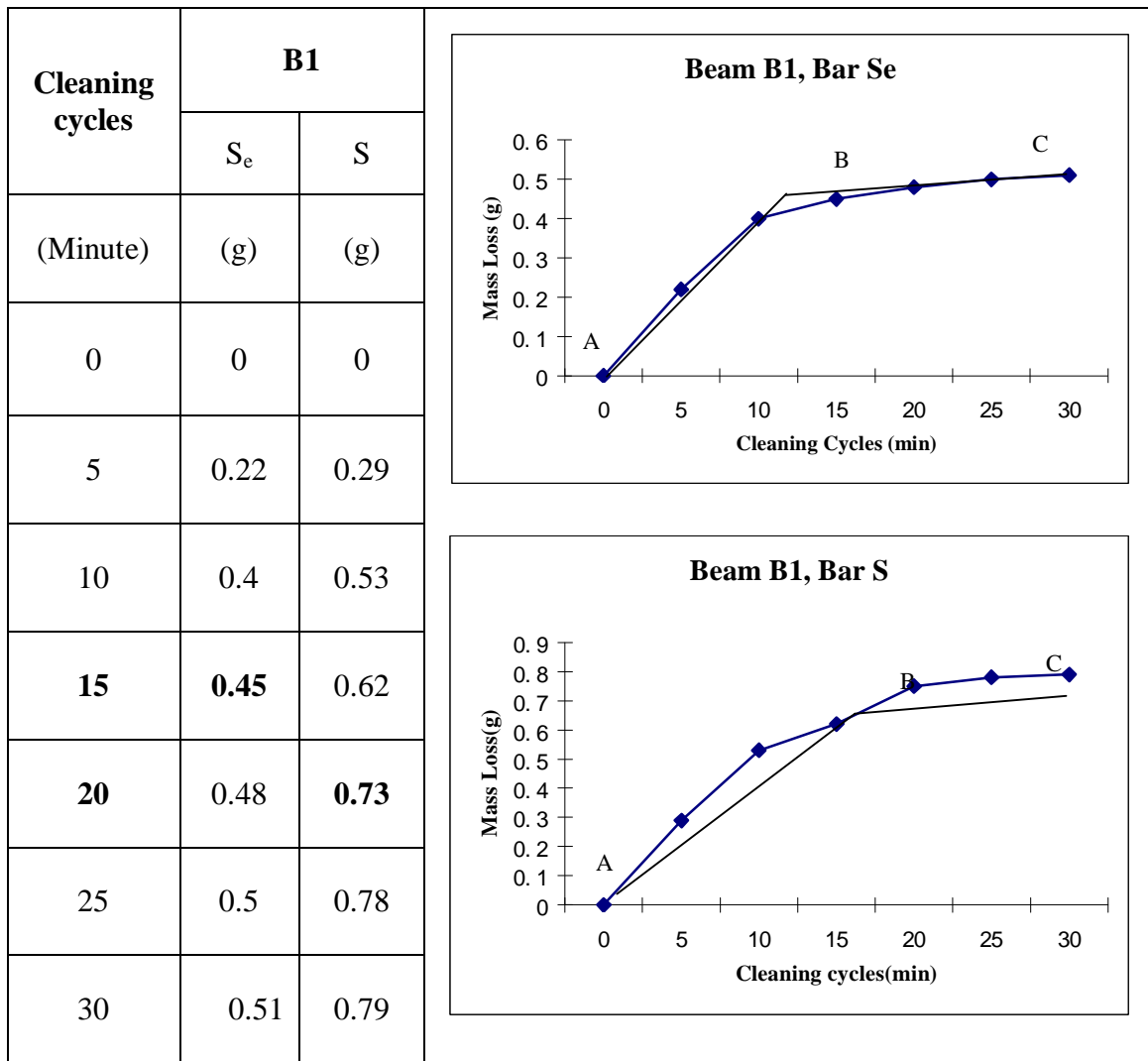


Cleaning cycles (Minute)	A2	
	S _e (g)	S (g)
0	0	0
5	0.29	0.35
10	0.61	0.77
15	0.82	0.98
20	0.87	1.08
25	0.89	1.14
30	0.9	1.16



Cleaning cycles (Minute)	A3	
	S _e (g)	S (g)
0	0	0
5	0.23	0.38
10	0.59	0.78
15	0.82	0.95
20	0.92	1.06
25	0.96	1.1
30	0.97	1.12





Cleaning cycles (Minute)	B2	
	S _e (g)	S (g)
0	0	0
5	0.29	0.25
10	0.53	0.52
15	0.62	0.62
20	0.75	0.67
25	0.78	0.68
30	0.79	0.69

